IEEE Access
Multidisciplinary | Rapid Review | Open Access Journal

Received 4 July 2023, accepted 27 July 2023, date of publication 2 August 2023, date of current version 8 August 2023.

Digital Object Identifier 10.1109/ACCESS.2023.3301148

TOPICAL REVIEW

A Comprehensive Review on Flywheel Energy Storage Systems: Survey on Electrical Machines, Power Electronics Converters, and Control Systems

REZA TAKARLI[1], (Student Member, IEEE), ALI AMINI[1], MOHAMMADSADEGH KHAJUEEZADEH[1], MOHAMMAD SHADNAM ZARBIL[1], ABOLFAZL VAHEDI[1], (Senior Member, IEEE), ARASH KIYOUMARSI[2], HADI TARZAMNI[3], (Student Member, IEEE), AND JORMA KYYRA[3], (Member, IEEE)

[1]Department of Electrical Engineering, Iran University of Science and Technology (IUST), Tehran 1684613114, Iran
[2]Department of Electrical Engineering, Faculty of Engineering, University of Isfahan, Isfahan 8174673441, Iran
[3]Department of Electrical Engineering and Automation, Aalto University, 02150 Espoo, Finland

Corresponding author: Hadi Tarzamni (hadi.tarzamni@aalto.fi)

This work was supported by the Finnish Electronic Library (FinELib), Finland, through the FinELib consortium's agreement with the Institute of Electrical and Electronics Engineers (IEEE).

ABSTRACT Finding efficient and satisfactory energy storage systems (ESSs) is one of the main concerns in the industry. Flywheel energy storage system (FESS) is one of the most satisfactory energy storage which has lots of advantages such as high efficiency, long lifetime, scalability, high power density, fast dynamic, deep charging, and discharging capability. The above features are necessary for electric vehicles (EVs), railways, renewable energy systems, and microgrids. Also, electrical machines, power electronics converters, and control systems are the cores of energy transfer in FESS. Therefore, they have a critical role in determining efficiency, power rating, power factor, cost, angular velocity, and volume of FESS. So, in this study, the FESS configuration, including the flywheel (rotor), electrical machine, power electronics converter, control system, and bearing are reviewed, individually and comprehensively. Additionally, the mentioned components have been categorized to be a guide for future research. The investigated electrical machines are compared by Finite Element Analysis (FEA). Subsequently, our laboratory's measurement results are reviewed experimentally showing the progress in the field of FESS, such as designing robust control algorithms and an Interior Permanent Magnet-Synchronous Reluctance Machine (IPM-SynRM) to use in FESS.

INDEX TERMS Energy storage system (ESS), flywheel energy storage system (FESS), electric machine, power electronics converter, control system, finite element analysis (FEA).

ABBREVIATION

3D	Three-Dimensional.
ACHM	AC Homopolar Machines.
AMB	Active Magnetic Bearings.
A-PMB	Attractive Passive Permanent Magnetic Bearing.
BBLDCM	Bearingless Brushless Direct Current Machine.
BES	Battery Energy Storage.
BLDCM	Brushless DC Machines.
BPMSM	Bearingless Permanent Magnet Synchronous Machines.
BSRM	Bearingless Switched Reluctance Machine.
BTB	Back-to-Back.
CAES	Compressed Air Energy Storage.

The associate editor coordinating the review of this manuscript and approving it for publication was Alexander Micallef.

CCS	Continuous Control Set.
CPWSR	Constant-Power Wide-Speed Range.
DFIM	Double-Fed Induction Machine.
DMC	Direct Matrix Converter.
DPMSM/G	Double-side Permanent Magnet Synchronous Motor/Generator.
DTC	Direct Torque Control.
ESS	Energy Storage System.
EV	Electric Vehicle.
FCS	Finite Control Set.
FEA	Finite Elements Analysis.
FESS	Flywheel Energy Storage System.
FIR	Finite Impulse Response.
FOC	Field-Oriented Control.
GES	Gravity Energy Storage.
GSC	Grid-Side Converters.
HESS	Hydrogen Energy Storage System.
HIA	Homopolar Inductor Alternator.
HPF	High Pass Frequency.
HSFESS	High Rotation Velocity.
HSM	Homopolar Synchronous Machine.
IM	Induction Machines.
IMC	Indirect Matrix Converters.
IPM	Interior PM.
LSFESS	Low Rotation Velocity.
MIMO	Multiple Input/Multiple Output systems.
MPC	Model Predictive Control.
MSC	Machine-Side Converters.
MTPA	the Maximum Torque Per Ampere.
NPC	Neutral Point Clamped.
P-Boost	Plus Boost.
PHES	Pumped Hydro Energy Storage.
PMa-SynRM	Permanent Magnet Assisted Synchronous Reluctance Machine.
PMB	Passive Permanent Magnetic Bearings.
PMSM, ACHM	Permanent Magnet Synchronous Machines.
PMSM/G	PMS motor/generator.
P-NPC	Plus NPC.
PWM	Pulse Width Modulation.
R-PMB	Repulsive Passive Permanent Magnetic Bearing.
RPWV	Rectangular Pulse Waves.
SCES	Super-Capacitors Energy Storage.
SMB	Superconducting Magnetic Bearings.
SMES	Superconducting Magnetic Energy Storage.
SRM	Switched Reluctance Machines.
SynRM	Synchronous Reluctance Machines.
TES	Thermal Energy Storage.
THD	Total Harmonic Distortion.
UPS	Uninterrupted Power Supply.
VAI	Volt-Ampere Inverter.
VFD	Variable Frequency Drive.
ZSC	Z-source Converter.

I. INTRODUCTION

The usage and development of Energy Storage Systems (ESSs) have been increased to balance the supply and demand of electrical energy sources [1]. Hydrogen Energy Storage System (HESS) [2], Battery Energy Storage (BES) [3], Compressed Air Energy Storage (CAES) [4], Super-Capacitors Energy Storage (SCES) [5], Superconducting Magnetic Energy Storage (SMES), Thermal Energy Storage (TES) [6], Pumped Hydro Energy Storage (PHES) [7], Gravity Energy Storage (GES) [8], and Flywheel Energy Storage System (FESS) are among most known EESs in electric systems. The storing and retrieving of energy must be at longer timescales if supply and demand do not match. A fast dynamic is unnecessary here if other technologies have already met this feature. i.e., a PHES gives a few hours of storage but takes time to reach the full of energy. It must therefore be used in coupling with a fast dynamic technology in the grid system, such as BES or FESS. Accordingly, comparing the energy storage system technologies based on dynamic and duration is shown graphically in Fig. 1. According to Fig. 1, FESS, BES, and SCES are the main rivals [1]. BES is usually used for high-energy capacity purposes. However, BES has low reliability, high sensitivity to heat, a short life cycle, high cost, and high maintenance cost [9]. Also, unlike BES, FESS is suitable for high charging and discharging rates with a high power rate [1]. SCESs are used when many fast charge/discharge cycles are mandatory. However, the energy capacity of the SCESs is low [5]. Additionally, SCES has disadvantages such as low energy density, high self-discharge loss, and a short storage cycle [5], [10]. According to [10], the energy density of FESS, SCES and Li-ion BES are 5-100 Wh/kg, 2.5-50 Wh/kg and 150-350 Wh/kg, respectively. Also, the total capital cost, per unit of the power rating of FESS, SCES and Li-ion BES are 590-1446 €/kW, 774-914 €/kW and 2109-2746 €/kW, respectively.

FESS, a so-called mechanical battery, is one of the most common and oldest ESSs [11]. The FESS has two main tasks, storing the kinetic energy of a rotary disk (charging mode), which has a coupling with the electrical machine's shaft, and releasing the stored energy in the grid (discharging mode) at a necessity [12]. In charging mode, FESS stores kinetic energy by a motor. During discharge, the same motor acts as a generator that generates electricity from the rotary energy of the flywheel disk [13]. configurations of the FESS are simpler than the other energy storage, in which its storing and releasing cycles have no constraints. The advantages of FESS are high efficiency, long lifetime, scalability, few environment contaminations, high power density, fast dynamic, and high charging/discharging capability [14], [15]. FESS is generally used in electric vehicles (EVs) [15], [16], [17], [18], railways [19], [20], [21], and renewable energy systems, including wind power generation systems [22], [23], [24], [25], [26], [27], microgrids [28], [29], and power quality such as frequency and voltage regulation [30], and Uninterrupted Power Supply

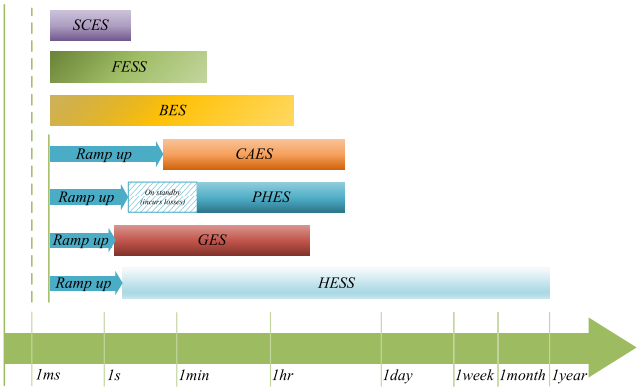

FIGURE 1. Comparing the energy storage system technologies based on dynamic and duration [14].

(UPS) [31], [32]. Accordingly, the FESS usages in EVs, UPS, and microgrids AC are shown in Fig. 2. Also, a laboratory model of the FESS which is from our laboratory is shown in Fig. 3. In different areas of grid storage such as power quality, frequency regulation, and balance, voltage sag control, and mitigation of grid voltage reduction, the flywheel system is widely used owing to its fast charging-discharging capability [33], [34]. Also, the system stability is disturbed by the emergence of renewable energy sources such as wind and solar energy. In wind energy systems, a flywheel system is used to correct wind oscillations and system frequency balance, while in solar energy systems, FESS is utilized in combination with batteries, which increases the system's efficiency and battery life [35].

The rotor's size and the rotation velocity affect the FESS's total energy. Moreover, the used electrical machine and its power factor affect the FESS's power rating and active power, respectively. Since FESS is often used in high rotation velocity, the chosen electrical machine must be eligible for this operating condition. One of the significant factors in choosing an ESS is cost; in FESS, the total cost relies on the electrical machine's cost. Moreover, efficiency is the other significant factor of these systems. The efficiency of the electrical machines has the most effect on the efficiency of FESS. Accordingly, the design of an electrical machine with lower losses while having high rotation velocity and cost-effectiveness is the priority in FESS. Hence, the electrical machine has a key role in determining the FESS's property and is the main core of transferring energy, which power electronics converters and control systems can aid it in a better mission. Thus, presenting a review to investigate the used electrical machines, power electronics converters, and control systems in FESS was necessary as a guide for the engineering community. Still, no review study has not been investigated the details of FESS configuration, especially electrical machines. i.e., [36] and [37] gives a general view of FESS but not a detailed study. Reference [38] is a review of the FESS usage in power systems and microgrids. In [39] and [40], compared electrical machines used in FESS are very

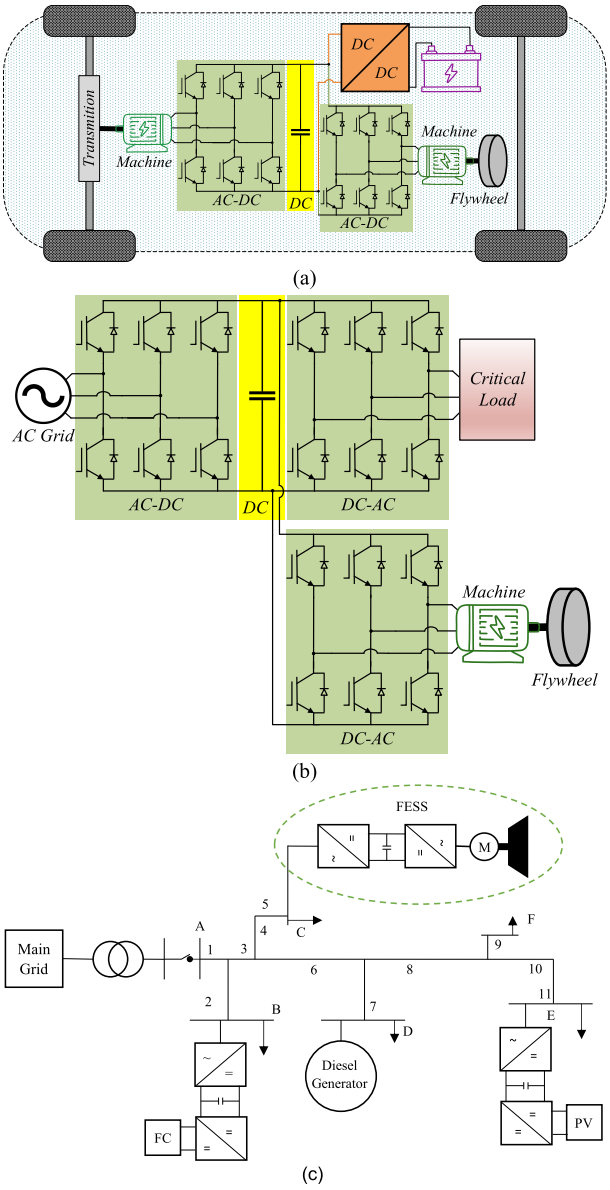

FIGURE 2. Flywheel energy storage system (FESS) usage in: (a) Electric Vehicles (EVs) and (b) Uninterrupted Power Supply (UPS), and (c) Microgrid (AC).

limited. Thus, the following review study fills a gap in the literature, and the main contributions are:

- Review of flywheel energy storage system configuration, separately and comprehensively, including different categories of electrical machines, power electronics converters, control system strategies, and bearings.
- Comparing the finite element analysis of the used electrical machines, regarding the usage metrics of the flywheel energy storage system.
- Review of the laboratory progress in the field of flywheel energy storage systems, including proposing robust control algorithms and designing the IPM-SynRM configuration.

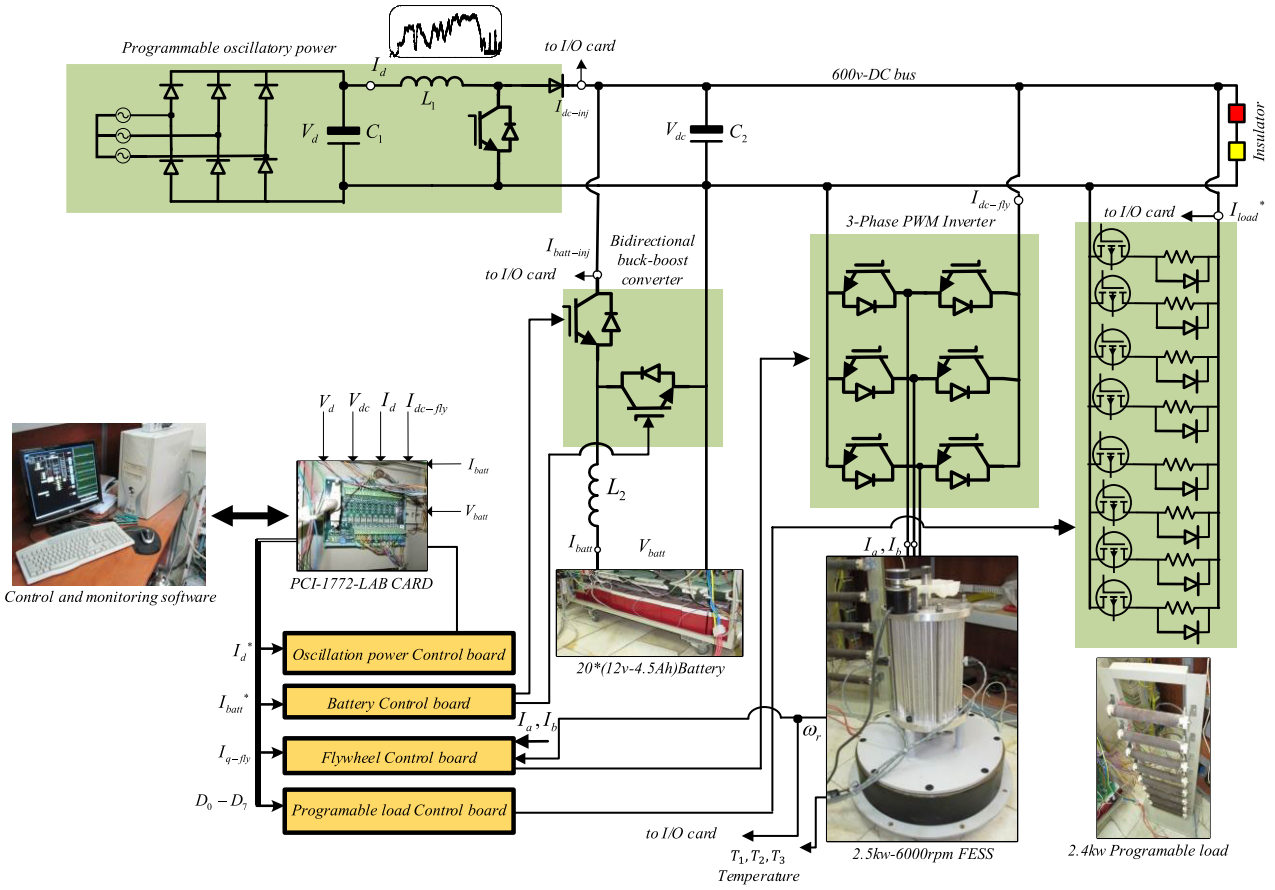

FIGURE 3. A laboratory model of the Flywheel energy storage system.

In Fig. 4 a chronological diagram is shown by presenting the most effective and well-known research in each of the surveyed fields including electrical machines, power electronics converters, control systems, and bearings.

In this study, at first, the FESS configuration, including flywheel (rotor), electrical machine (motor/generator), power electronics converters, control systems, and bearings, are investigated comprehensively. Then, compared electrical machines are verified by the Finite Elements Analysis (FEA). Finally, the review of our laboratory works in the FESS field, including the design of a robust control system and Permanent Magnet Assisted Synchronous Reluctance Machine (PMa-SynRM) to use in FESS, is done. An overview of the review methodology and details of each section are displayed in Fig. 5.

II. FLYWHEEL ENERGY STORAGE SYSTEM CONFIGURATION

Fig. 6 demonstrates the main configuration of the FESS including a flywheel (rotor), electrical machine (motor/generator), power electronics converters, control system, and bearing. The FESS has three operating modes, including charging mode (storing energy), standby mode (keeping energy), and discharging mode (releasing energy). FESS receives energy from an electrical source, such as the grid in charging mode. In charging mode, the higher kinetic energy is yielded by increasing the flywheel's angular velocity (rotor), storing the electrical energy in the form of mechanical energy in the flywheel (rotor). In charging mode, the electrical machine acts in motor mode using a power electronics converter and control system, as shown in Fig. 7(a). In standby mode, the flywheel (rotor) must stay at an almost constant angular velocity, as shown in Fig. 7(b). In the discharge mode, the flywheel's angular velocity (rotor) goes down, and kinetic energy converts into electrical energy. In discharge mode, the electrical machine acts as a generator, supplying the grid or loads through the power electronics converters, as shown in Fig. 7(c). Accordingly, the electrical machine and its control system are the main core of transferring energy in FESS. Fig. 8 is displayed for comprehending the FESS operating modes, including charging (storage), standby (keeping), and discharge (releasing) [14]. In the following, the main configuration of the FESS is investigated individually, such as flywheel (rotor), electrical machine (motor/generator), power electronics converters, control system, and bearing. The changes in flywheel angular velocity and energy under different operating modes such as charging, standby, and discharging can be shown in Fig. 9.

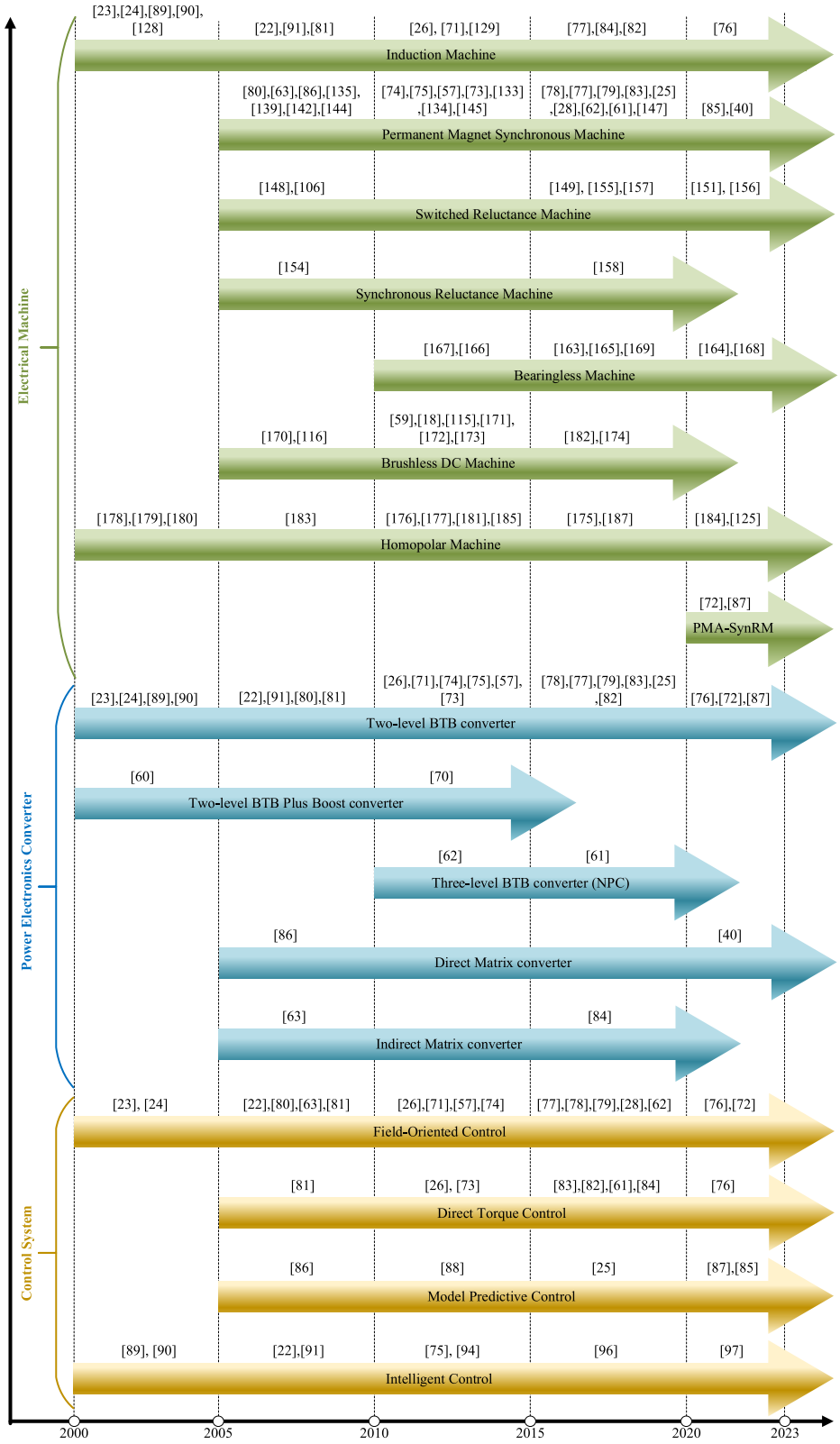

FIGURE 4. A chronological diagram by presenting the most effective and well-known research in each of the surveyed fields including electrical machines, power electronics converters, control systems, and bearings.

FIGURE 5. An overview of the review methodology and details of each section.

A. FLYWHEEL (ROTOR)

A flywheel (rotor) is a rotating disk that stores mechanical energy. The stored energy in the flywheel is as follows:

$$E = \frac{1}{2} J \omega^2 \tag{1}$$

where E is the stored kinetic energy, J is the moment of inertia in the flywheel, and ω is its angular velocity [14], [41]. According to (1), energy can be higher by increasing the angular velocity or increasing the moment of inertia. It brings two choices for FESS, FESS with low rotation velocity (LSFESS) and FESS with high rotation velocity (HSFESS). The LSFESS is made from steel and has more weight with less cost than HSFESS [42], [43], [44]. The flywheel's size, form, and mass (rotor) affect the moment of inertia. In general, the rotor is a solid cylindrical object. J is written as below:

$$J = \frac{1}{2} m r^2 = \frac{1}{2} \rho a \pi r^4 \tag{2}$$

where m is mass, r is the radius, a is the length, and ρ is mass density. it is noteworthy that, more energy can be stored by using materials with higher mass density or by increasing the disk radius [14]. The flywheel's function can be simplified as follows:

$$J \frac{d\omega}{dt} = T_{em} - f\omega \tag{3}$$

where T_{em} is the electromechanical torque and f is the friction coefficient.

B. ELECTRICAL MACHINE (MOTOR/GENERATOR)

The electrical machine has a key role in FESS. Using a control system appropriately transfers energy between the motor and

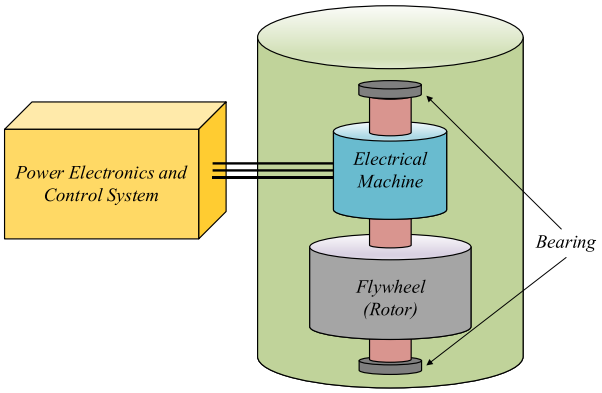

FIGURE 6. Overview of FESS configuration, including flywheel (rotor), electrical machine (motor/generator), power electronics and control system, and bearing.

generator modes. The electrical machine is an electromechanical interface in FESS that converts electrical energy into mechanical energy and vice versa [45]. In storing mode, the electrical machine must act as a motor, and by increasing the flywheel's angular velocity (rotor), the electrical energy will be stored as kinetic energy. In releasing mode, the electrical machine must act as a generator; so, by decreasing the flywheel's angular velocity (rotor), the kinetic energy converts into electrical energy [14], [39], [40], [46], [47]. The electrical machine's size and cost rely on T_{em}. The rotation velocity range of the flywheel (rotor) must be between a minimum and maximum value, which causes a satisfactory value of T_{em}. The capacity of storing or releasing energy by FESS can be shown as follows:

$$\Delta E = \frac{1}{2}J\left(\omega_{max}^2 - \omega_{min}^2\right) = \frac{1}{2}J\omega_{max}^2\left(1 - \frac{\omega_{min}^2}{\omega_{max}^2}\right) \quad (4)$$

While ω_{min} is usually set between one third and one half of ω_{max}. Choosing $\omega_{min} = 1/3\omega_{max}$ makes the electrical machine 50% larger than when $\omega_{min} = 1/2\omega_{max}$, but more energy extraction is yielded from the flywheel (rotor). So, a trade-off must be chosen in the angular velocity range. Keeping this fact in mind that, for low-power machines, as the flywheel (rotor) brings the highest cost to the FESS, a system with lower ω_{min} will be chosen for increasing the usable capacity. Correspondingly, the contrary is true for high-power machines [14]. Electrical machines, including Induction Machines (IM), Permanent Magnet Synchronous Machines (PMSM), Switched Reluctance Machines (SRM), and Synchronous Reluctance Machines (SynRM), are the most common electrical machines used in FESS. Brushless DC Machines (BLDCM), AC Homopolar Machines (ACHM), and Bearingless machines are among the other electrical machines to use in the FESS.

In HSFESS, both the electrical machine and the flywheel are fully integrated. In LSFESS, they are partially integrated into the housing box or will be employed separately [27]. In Table 1, the LSFESS and HSFESS are investigated against each other [14], [27], [44], [48], [49], [50].

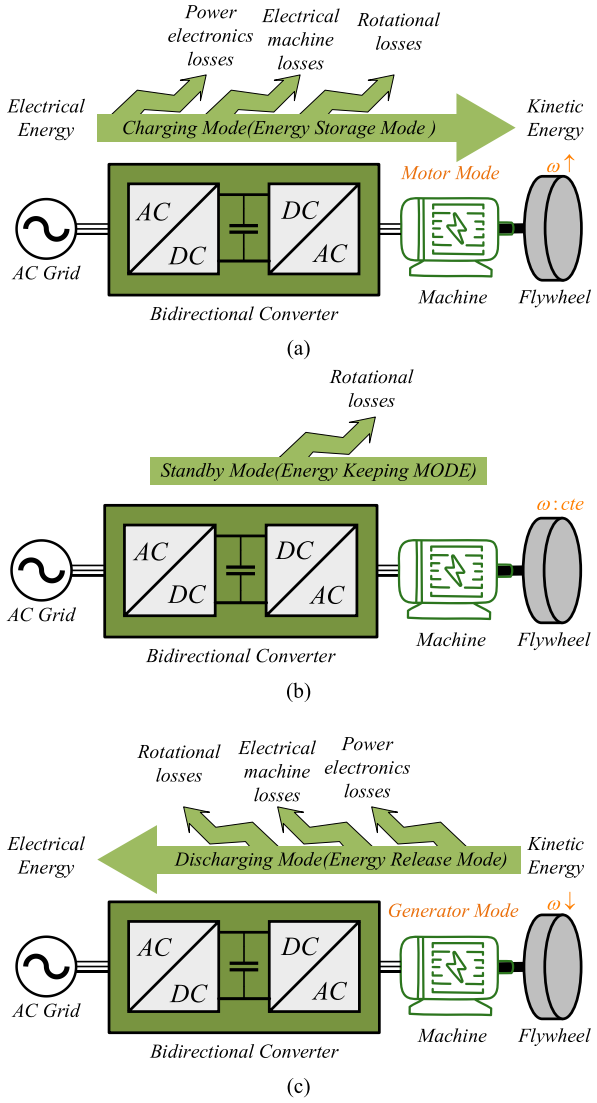

FIGURE 7. Three operating modes, including (a) charging mode (storage energy mode), (b) standby mode (keeping energy mode), and (c) discharging mode (releasing energy mode).

C. POWER ELECTRONICS CONVERTERS AND CONTROL SYSTEMS

Power electronics converters are the link between the electrical machine and the electrical load/supply, which play a significant role in the satisfactory performance of electrical machines. Using control of the electrical machine, energy transfers between the FESS and the electrical load/supply [1], [36], [51]. Increasing the switching frequency in power electronics converters has advantages, such as increasing the rectifier control bandwidth and reducing Current Ripple (I_{ripple}). On the other hand, increasing the switching losses is often a disadvantage [44], [52]. The electrical machine acts as a generator or a motor based on the situation by controlling power electronics converters. The most common power electronics converters used in the FESS to control electrical machines are AC-DC-AC

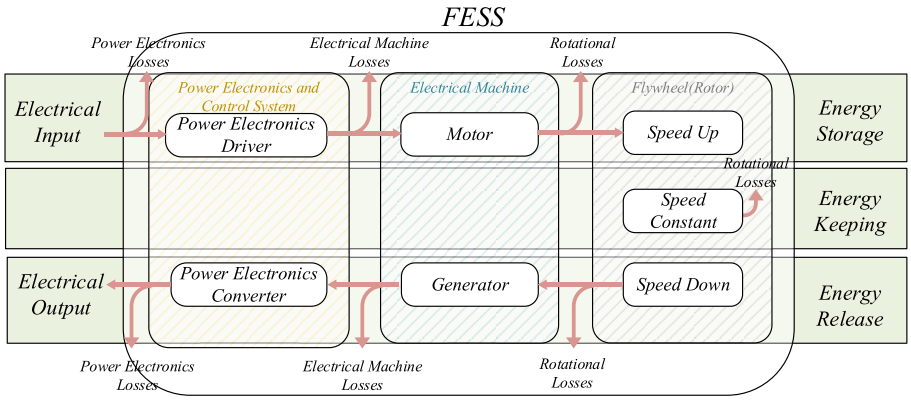

FIGURE 8. Comprehending the FESS operating modes, including charging (storage), standby (keeping), and discharge (releasing).

TABLE 1. Comparing the LSFESS and the HSFESS against each other [14], [27], [44], [38], [49], [50].

Characteristic	*Low-Speed FESSs (LSFESS)*	*High-Speed FESSs (HSFESS)*
Flywheel (Rotor) Material	Steel	Composite
Electrical Machine	IM , PMSM , SynRM , SRM	PMSM , SynRM , SRM
Integration of Electrical Machine and Flywheel	No Integration or Partial Integration	Full or Partial Integration
Bearings	Mechanical or Mixed (Mechanical and Magnetic)	Magnetic
Cost	Low	High

(back-to-back) and AC-AC converters. Back-to-Back (BTB) converters contain a DC link and two converters on both sides. These converters are Machine-Side Converters (MSC) and Grid-Side Converters (GSC) [53], [54], [55], [56], [57]. In BTB converters, the GSC converts AC voltage to DC voltage, and then MSC converts DC voltage to an arbitrary AC voltage and frequency. A two-level BTB is shown in Fig. 10(a). The MSC controls the angular velocity and flux, owing to control of the FESS active power; subsequently, the GSC controls the DC link voltage [36]. In BTB converters, the control of switches is often by the Pulse Width Modulation (PWM) strategy. The PWM strategy uses Rectangular Pulse Waves (RPWV) and adjusts their width. The RPWV controls the converter in generating an AC voltage sinusoidal from the DC link, leading to control of the electrical machines for operating appropriately in the FESS [35], [44], [58]. Adding a DC-DC stage between the AC-DC and DC-AC stages obtains more satisfactory operating conditions in the BTB converters. Accordingly, as shown in Fig. 10(b), a boost converter can be used to adjust and boosts the voltage when the angular velocity of the flywheel is low [59], [60]. Owing to the high voltage challenges in conventional two-level BTB converters, multilevel converters such as Neutral Point Clamped (NPC) can be used, which gives advantages such as higher efficiency, the smaller size of filter elements, lower harmonic orders, lower voltage stress on switches and the lower common-mode voltages. On the contrary, the higher number of switches will bring higher costs. Fig. 10(c) shows the NPC three-level BTB used in FESS. In the NPC three-level BTB converter, besides the DC-link voltage control, the voltage balance control of capacitors is also necessary [61], [62]. The BTB converter topologies have disadvantages owing to the DC-link capacitor, which brings a shorter system lifetime and makes the converter bulky and heavy, increasing maintenance costs. Accordingly, the AC-AC converters or Direct Matrix Converter (DMC), without a DC-link capacitor and consequently no large size, can be regarded to overcome the above challenges. The DMC is an array of nine switches bidirectionally arranged to give the connection capability between output and input, one by one. The matrix converters have disadvantages such as the voltage gain constraint, high Total Harmonic Distortion (THD), and more control complexity [63], [64], [65]. The matrix converters can be categorized into Direct MC (DMC) and Indirect Matrix Converters (IMC). Therefore, to overcome the voltage gain constraint, IMCs can be regarded. The IMC and DMC are shown in Fig. 10(d) and Fig. 10(e), respectively. In IMCs, the voltage gain will be boosted in reverse mode when the generator's output voltage is low, owing to the low angular velocity of the flywheel [66], [67]. Other converter categories have been used to control the drive of electrical machines in FESS, including Z-source Converter (ZSC) [45], [68], [69], boost DC/AC converter [70], and DC-DC Plus NPC (P-NPC) [62]. Whereas the most used converters for electrical

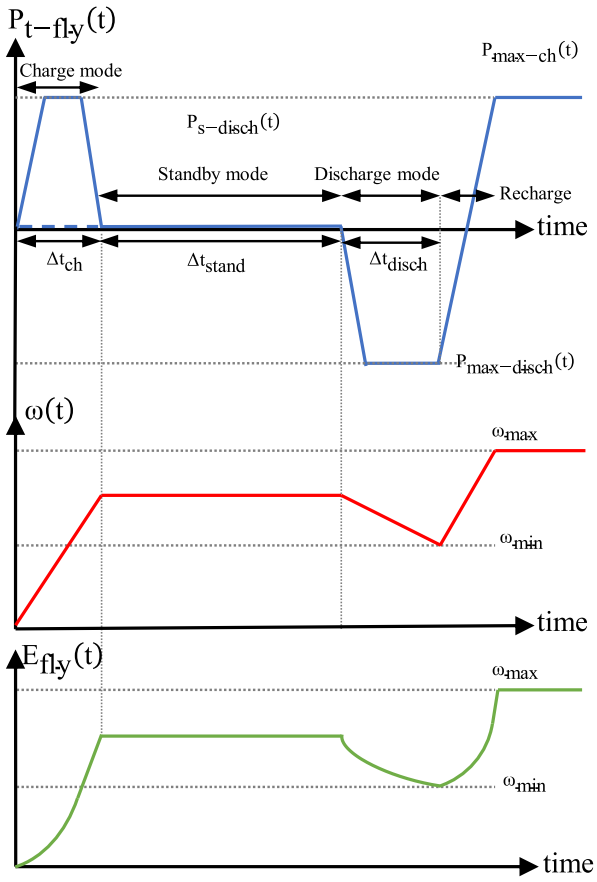

FIGURE 9. The changes in flywheel's active power, angular velocity, and energy under different operating mode conditions such as charging, standby, and discharging.

machines' drives in FESS are; two-level BTB, two-level BTB Plus Boost (P-Boost), NPC three-level BTB, DMC, and IMC. Comparing the above converters is displayed in Table 2 [39], [40].

In practical operations, the FESS must demonstrate a superior level of performance, including a smooth and rapid charging process, effective dynamic response capability through the discharging process, and anti-interference ability during both the charging and discharging process. Hence, The power electronic converter's control performance plays a critical role in achieving these goals [59]. Generally, most of the Variable Frequency Drive (VFD) control strategies can be employed to apply MSC control in FESS [25], [26], [71], [72], [73], [74], [75], [76], [77], [78], [79], [80], [81], [82], [83], [84], [85], [86], [87], [88], [89], [90], [91], [92], [93], [94], [95], [96], [97]. However, designing controllers for FESS requires taking into account some differences and peculiarities compared to VFD control. One of the challenges in FESS control is maintaining the desired voltage for the load during discharging mode, which involves dealing with nonlinearities, disturbances, and uncertain factors. The DC-link controller needs to be robust against these factors to ensure consistent performance. While most literature focuses on charging control strategies for FESS, there is limited work on discharging control techniques. For example, in reference [59], the main contribution of the authors was to study the FESS discharge control of the Buck-boost converter But, considering the wide-range speed variation effect, which is crucial to determine the energy storage capacity and discharge depth of a FESS, has been ignored. In [79], a discharge strategy that can consider the wide range of speed variation and maintain robust discharge performance is presented. However, this strategy does not control the inner current loop. To consider consistent fast dc-link voltage dynamic performance for the HSFESS, a fast dc-link voltage strategy based on a global linearization model and a linear extended state observer is proposed in [78]. In FESS, since the rotation velocity of the flywheel (rotor) is very high, especially in systems with magnetic bearings, sensorless control is more attractive; without the challenges of rotor angle extraction in the higher rotation velocity. Moreover, while fast charging and discharging are out, it is necessary to use smooth transition control between charging and discharging to avoid disturbances in transients. Accordingly, the most common strategies of MSC control are Field-Oriented Control (FOC), Direct Torque Control (DTC), Model Predictive Control (MPC), and intelligent control. Comparing the above control strategies is displayed in Table 3, according to the electrical machine and power electronics converter. Based on Table 3, the FOC control strategy, the two-level BTB, and IM or PMSM have more employed [40].

D. BEARINGS

Bearings are responsible for providing minimum friction drag for the electrical machine and the flywheel (rotor) [98]. Friction, loss, and cost tightly rely on the bearings' design. So, a weak bearing design brings more friction, losses, and more maintenance costs [14], [37], [99], [100]. In general, the bearings can be categorized as mechanical and magnetic. Mechanical bearings are usually employed for LSFESS with low rotation velocity, giving advantages such as lower initial cost and easy mounting. On the contrary, it brings some disadvantages, such as high friction and losses, requiring lubrication and maintenance, and a shorter lifetime [14], [38], [48], [101], [102]. A rolling element bearing is shown in Fig. 11(a) as a mechanical bearing. Although rolling element bearing friction is low over the other mechanical bearings, leading to higher losses. So, rolling element bearings are usually employed in conjunction with magnetic bearings. After the emerging magnetic bearings, the FESS industry has fundamentally changed. Magnetic bearings have advantages such as a longer lifetime, higher rotation velocity, higher load capacity, and higher dynamics. Nevertheless, it brings more complexity to the control system [103], [104]. Magnetic bearings are categorized as Passive Permanent Magnetic Bearings (PMB), Active Magnetic Bearings (AMB), and Superconducting Magnetic Bearings (SMB).

TABLE 2. Comparing common PE converters employed in FESS to control the electrical machine [39], [40].

Topologies	*No. Of Switches*	*No. Of Diodes*	*Features*	*Limitations*
Two Level BTB Fig. 10(a)	12	12	• Widely used • Mature control and modulation strategies • Bidirectional power flow	• Need DC voltage control • Bulky DC-link capacitor • Limited voltage boost capability
Two Level BTB + Boost Fig. 10(b)	13	13	• Voltage boost capability • Bidirectional power flow	• Need DC voltage control • Bulky DC-link capacitor
NPC Three-Level BTB Fig. 10(c)	24	36	• Multi voltage levels • High power quality • Bidirectional power flow • Low total harmonic distortion • Less voltage stresses	• Need DC voltage control • High cost • A large number of devices • Bulky DC-link capacitor • Need balancing control of capacitors
Indirect Matrix Converter Fig. 10(d)	18	18	• High efficiency • Direct AC/AC conversion • No bulky DC-link capacitor • Compact size • Indirect conversion • Low-maintenance • Controllable input power factor • No Requirement for DC voltage control • Bidirectional power flow	• High dependency of output from input • A large number of devices • Complex commutation
Direct Matrix Converters Fig. 10(e)	18	18	• High efficiency • Direct AC/AC conversion • No bulky DC-link capacitor • Compact size • Direct conversion • Low-maintenance • Controllable input power factor • No Requirement for DC voltage control • Bidirectional power flow	• Complex commutation • A large number of devices • High dependency of output from input • Limited voltage transfer ratio

1) PERMANENT PASSIVE MAGNETIC BEARINGS (PMB)

A PMB system has no external controls and consists of PMs, which gives the rotation capability to the flywheel (rotor). On the contrary, it should be employed along with other bearings owing to low stability. PMB has the advantages of high stiffness, low cost, and low losses owing to the lack of a current. Although it has low damping capability and no active control [105], [106], [107], [108]. It can be categorized as Repulsive Passive Permanent Magnetic Bearing (R-PMB) and Attractive Passive Permanent Magnetic Bearing (A-PMB); in the axial or radial installation. A PMB consists of two annular magnets, which are magnetized in a coaxial direction, as shown in Fig. 11(b). It is stable since reducing the gap between them increases the force. However, the bearing is unstable in radial mounting. So, requiring the radial bearings with radial stiffness greater than the anti-stiffness of the axial bearing. Using two rolling element bearings to maintain the radial location of a vertical shaft and use an R-PMB to handle the weight. On the other hand, an A-PMB can eliminate the second magnet that would have to be used on the rotor, in the case of R-PMB, as shown in Fig. 11(c). Although the radial anti-stiffness is also lower, this bearing is unstable, given the increasing axial attractive force with a reducing gap. The A-PMB tends to work best in conjunction with rolling element bearings, which can also take a share of the axial load. The radial PMB, Fig. 11(d), has stacks of annular magnets on both the shaft and the stator, while the fields of all magnets are aligned radially. Accordingly, the annular magnets in the gap keep the shaft centrally aligned. On the other hand, the shaft will move axially without axial constraints, leading to instability [14], [109].

2) ACTIVE MAGNETIC BEARINGS (AMB)

AMB has windings whose currents can adjust the amount of electromagnetic force in the system, reducing rotor vibrations and excluding their losses. Adjusting is through a rotor angle feedback controller. A radial AMB is shown in Fig. 11(e). The bearing restoration force is controlled by changing the current in the stationary coils. Although it has control complexity, using such bearings is attractive, given bearing maintenance can be significantly lower against the rolling element bearings that suffer from wear and fatigue. The axial AMB can also be used, Fig. 11(f), requiring coils on either side of a disc that can only attract the disc. So, it works similarly to the radial one, the attraction of the side that is moving away [14]. AMB has the advantages of control ability, high stiffness, and long

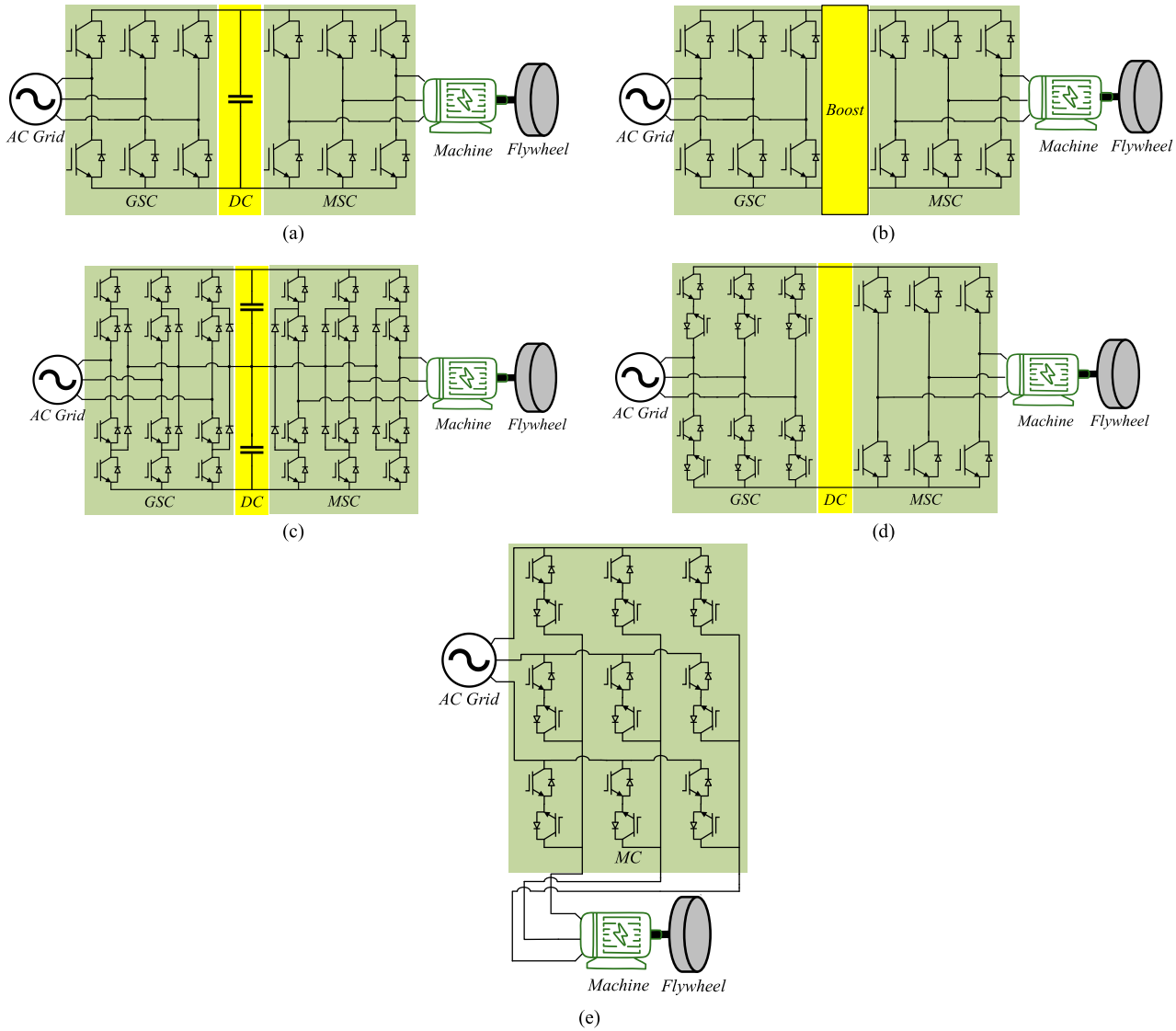

FIGURE 10. Common PE converters employed in FESS, including (a) Two-level BTB converter (b) Two-level BTB Plus Boost (P-Boost) converter (c) NPC three-level BTB converter (d) Indirect Matrix Converter (IMC) (e) Direct Matrix Converter (DMC).

lifetime, whereas it has disadvantages such as control system complexity, high cost, and losses owing to the current of the control system [14], [110], [111], [112], [113]. Using AMB and mechanical bearings simultaneously gives lower control complexity and more stability and affordability [39], [114].

3) SUPERCONDUCTING MAGNETIC BEARINGS (SMB)

SMB is based on superconductivity; Fig. 11(g) and 11(h) are for radial and axial mountings. Here, magnetic fields create currents in superconducting coils in the stator, repelling PMs on the rotor [14]. The SMB gives advantages such as high rotation velocity, no friction, long lifetime, less size, and stability. Accordingly, SMBs are eligible for HSFESS. The major disadvantage of the SMB is the necessity of a cryogenic cooling system to avoid the bearings' failure, which brings more cost to the SMB system. High-temperature superconductors can be employed to overcome the cooling system challenge in SMBs. Additionally, SMB and PMB can be used simultaneously to have a lower necessity for the cooling system and be more cost-effective [14], [115], [116], [117], [118], [119], [120]. Comparing the bearing categories is displayed in Table 4. Fig. 12 displays the main configuration of the FESS.

III. ELECTRICAL MACHINES CATEGORIES IN FESS

The following section reviews the electrical machines employed in FESSs. Whenever the electrical machine acts as a motor, the energy transferring, charging, and storing in the FESS will be yielded. On the other hand, when the FESS is discharging, the machine acts as a generator [37], [39]. Accordingly, the electrical machine has a key role in electrical and mechanical energy conversion and significantly affects

TABLE 3. Comparison of the Machine-Side Converter (MSC) control strategies in the FESS [39], [40].

Charging Control Strategies	*Advantages*	*Disadvantages*	*Controller Platform*	*Application*
FOC	• Good steady-state behavior • Relatively lower torque ripples • Mature and widely used • Fixed switching frequency	• Require coordinate transformation (*abc*↔*dq0*) • Relatively slower dynamics • Empirical design of PI parameters • Require modulation stage (e.g., SVM and SPWM)	• Two level BTB+IM [22]–[24], [26], [71], [76], [77], [81] • Two level BTB+PMSM [57], [74], [77]–[80] • Two level BTB+PMA-SRM [72] • Three level BTB(NPC)+PMSM [28], [62] • IMC+PMSM [63]	• EV [80] • MG [28] • WPGS [22]–[24], [26], [76], [81] • WPGS and AC MG [57], [62], [71], [74] • Dynamic voltage restorer [63] • Grid/Load support [72], [77], [78]
DTC	• control for low speeds • Simple and robust • Light computational burden • No modulation stages • Accurate speed and torque • Fast dynamics • No coordinate transformation	• Considerable torque ripples • Design of hysteresis band (the wider band, the higher switching frequency) • Variable switching frequency	• Two level BTB+IM [26], [76], [81] • Two level BTB+PMSM [73], [83] • Two level BTB+DFIM [82] • Three level BTB(NPC)+PMSM [61] • IMC+IM [84]	• Grid connection of renewables [61] • WPGS [26], [76], [81]–[84] • Fault ride through in MC [83]
MPC	• Able to compensate for control delay • simple implementation • Optimization control approach • Able to include constraints • No modulation stage • Flexibility in control	• High computation cost if too many switch states • Variable switching frequency • Affected from the system model	• Two level BTB+PMSM [25] • Two level BTB+ Axial flux PMSM [88] • Two level BTB+ PMA-SynRM [87] • MC-PMSM [86]	• Dynamic voltage restorer [86] • Grid connection [25] • Grid/Load support [85], [87], [88]
Intelligent Control	• No Requirement for a precise model • PI control parameters Optimization • Fault-tolerant • Intelligent control • Robust	• Require expert knowledge which is hard to obtain • Intricate and hard to implement • Might affect dynamics and control accuracy • Require large computation • Approximated accuracy • Require modulation stage (e.g., SVM and SPWM)	• Two level BTB+IM [22], [89]–[91] • Two level BTB+PMSM [75]	• DC grid power [91] • WPGS [22], [75] • WPGS and diesel generator [89], [90] • Grid/Load support [75] • EV [74]

the operating condition of the FESS [121]. The most common electrical machines employed in FESS are; Induction Machines (IMs), Permanent Magnet Synchronous Machines (PMSMs), Switched Reluctance Machines (SRMs), and Synchronous Reluctance Machines (SynRM) [35], [122]. The following section also reviews the BLDCM, AC Homopolar Machines (HM), and bearingless machines.

A. INDUCTION MACHINE (IM)

Since IM has a rigid configuration, low cost, high T_{em}, strength, and reliability, it can be regarded as the best choice for high-power usages [35], [123], [124]. On the contrary, the main challenges of IMs are rotation velocity constraints, the control drive complexity, and numerous costly maintenances [108]. The IM generally has lower efficiency than the PMSMs [125] and is not eligible for the HSFESS [91]. Accordingly, in [126], a new design model has been suggested to lower losses in FESS usage. Double-Fed Induction Machines (DFIMs) are also suggested to overcome the low rotation velocity disadvantage [117], [127], [128], [129], [130]. Moreover, DFIMs have advantages, including flexible control and low conversion rate, allowing them to have a smaller converter's size [131]. Although the IM has severe constraints, particularly in HSFESS, according to economic efficiency, it is used in LSFESS, and the DFIM is more attractive for HSFESS.

B. PERMANENT MAGNET SYNCHRONOUS MACHINE (PMSM)

PMSMs are satisfactory in FESS owing to their high power density and efficiency [35], [132], [133], [134], without requiring an external excitation current due to the magnetic

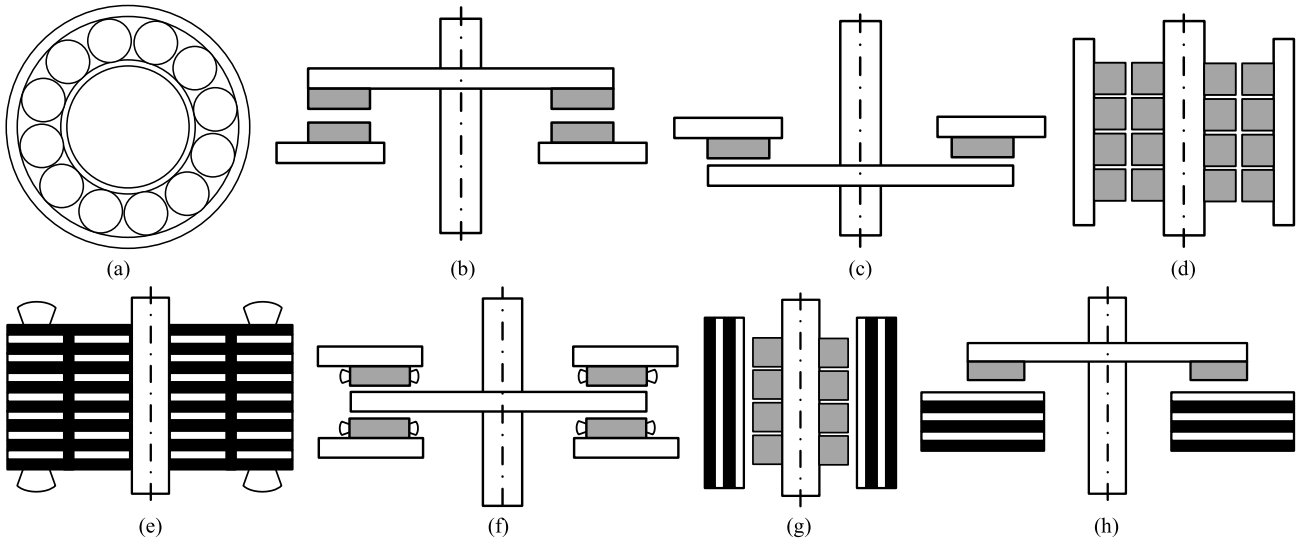

FIGURE 11. Bearings: (a) Rolling element (b) Passive magnetic axial repulsive (c) Passive magnetic axial attractive (d) Passive magnetic radial (e) Active magnetic radial (f) Active magnetic axial (g) Super conducting magnetic radial (h) Super conducting magnetic axial.

flux of PMs. Hence, PMSM gives a higher power factor, lower losses, and causes lower the necessity for Volt-Ampere Inverters (VAIs). However, PMSMs are subject to demagnetization due to having magnets, leading to more sensitivity and vulnerability to heat than IMs [24]. In the PMS motor/generator (PMSM/G), the stator core's iron loss is owing to the magnetic field change in the idling mode, which causes slows down the PMSM/G [135]. In general, PMSMs are used in the industry with high rotation velocity necessity [20], [114], [136], [137], [138], [139], [140]. Although it is used at high rotation velocity, the rotor's mechanical behavior has complexity due to the existence of magnets in the rotor configuration. References [124] and [141] are given an overview of PMSM design concerns to use in the FESS, especially for lower iron loss. Seok-Myeong Jang designed an iron lossless PMSM for high-power FESS [143]. In [144], the operating range of a Double-side Permanent Magnet Synchronous Motor/Generator (DPMSM/G) is investigated to use in a FESS. In [145], the study on FESS design and assessment is on reducing motor Torque Ripple (T_{ripple}) to ensure output power stability. In [146], a DPMSM/G is investigated in the FESS to lower the iron losses in idling mode.

C. SWITCHED RELUCTANCE MACHINE (SRM)

SRM has advantages, such as configuration simplicity and rigidness [147], [148] and less iron loss, as well as the ability to work in harsh environments and operating conditions [149]. Further, it has a wide rotation velocity range, high acceleration capability, high efficiency, simplicity in converter circuit design, and fault-tolerant ability [37]. Although the SRM has no magnet [150], [151], [152], its efficiency is analogous to and even higher than that of the IMs at high rotation velocity. Additionally, SRM is controlled easier at high rotation velocity than IMs [153]. In general, the absence of magnets in the rotor configuration of SRM causes core losses in the stator core, especially at high rotation velocity, much less than in a PM machine. Hence, the efficiency of this machine is relatively high. Contrary to all the SRM's advantages and its limited usage in the FESS [154], [155], [156], it has a high T_{ripple} and is not eligible for this aim.

D. SYNCHRONOUS RELUCTANCE MACHINE (SynRM)

SynRMs are employed as motors/generators in FESS due to zero spinning losses when the machine generates no T_{em}. Moreover, the design of SynRM's rotor can have satisfactory integrity in construction if the rotor saliency is made by alternating layers of magnetic and non-magnetic metals, which are bonded together by a high-strength bonding method [153]. The simplicity of configuration [157], high efficiency, high power capability, and low VAI are the most significant design concerns of motor/generator in FESS [158]. Ordinarily, in SynRM, power factor, rotation velocity range at constant power region, and dynamic of the motor rely directly on the saliency ratio, which can be used for proposing a motor design optimally [159]. Different rotor designs in SynRM have been suggested to earn a satisfactory saliency ratio, including the single barrier rotor, the axially-laminated rotor, and the transversally-laminated rotor. Fig. 13 shows the SynRM rotor configurations. The single barrier type has a low saliency ratio, weakening its operating condition. The axially-laminated type is the best choice regarding the saliency ratio, but due to the layered configuration of the rotor, the eddy current losses will be high. The transversally-laminated type is analogous to the IM in manufacturing and is satisfactory for high rotation velocity owing to the strength of the rotor. In the rotor configurations of the above types of SynRM, using radial and tangential blades ensures mechanical strength at high rotation velocity.

TABLE 4. Summary of the magnetic bearings' advantages and disadvantages.

Type of magnetic bearing	*Advantages*	*Disadvantages*
PERMANENT (PASSIVE) MAGNETIC BEARINGS (PMB)	• high stiffness • low cost • low losses	• low damping capability • no active control
ACTIVE MAGNETIC BEARINGS (AMB)	• control ability • high stiffness • long lifetime	• control system complexity • high cost • losses caused by the current of the control system
SUPERCONDUCTING MAGNETIC BEARINGS (SMB)	• high rotational velocity • no friction • long lifetime • compact • stability	• necessity of a cryogenic cooling system • high cost

On the contrary, increasing the blades' width, especially at high rotation velocity, grows the leakage flux and the magnetic current. Accordingly, in SynRM, a high saliency ratio causes a high power factor, reducing losses and the rated VA of the inverter for the electrical machine [139], [157].

E. BEARINGLESS MACHINE

Using a mechanical bearing in the FESS suffers challenges such as friction, wear, tear, and dust contaminations, limiting the system's rotation velocity and useful life [160], [161]. These challenges can be solved by using magnetic bearings, but the increasing size and cost of the whole system will yield. Therefore, electrical machines without bearings are more attractive. The FESS, which combines two modes, including magnetic gear and magnetic bearing, in one machine, uses a bearingless machine [162], [163], [164]. Conventional bearingless electrical machines such as Bearingless Permanent Magnet Synchronous Machines (BPMSM), Bearingless Switched Reluctance Machine (BSRM), and Bearingless Brushless Direct Current Machine (BBLDCM) are employed in the FESS. However, the rotation velocity regulation of BPMSM is not satisfactory [162], and an external excitation system for BSRM is necessary, which certainly makes the cost and complexity higher [164], [165]. BBLDCM has advantages such as high rotation velocity, high reliability, wide rotation velocity regulation range, no mechanical friction, and no excitation, which make it attractive for FESS [166]. According to the above BBLDCM's advantages, its usage in the FESS is regarded [167]. Accordingly, in [168], an outer rotor BBLDCM is suggested for the FESS.

F. BRUSHLESS DC MACHINE (BLDCM)

BLDCMs are highly efficient, with many advantages such as high power density, high efficiency, relatively wide rotation velocity range, mechanical stability, low maintenance cost, and no Electromagnetic Interference (EMI) [59], [115], [169], [170], [171], [172]. However, BLDCM no-load losses are usually significant at high rotation velocity. Moreover, unbalanced forces during no-load bring high necessity conditions and obligations to the bearing capacity and stiffness of the magnetic bearing system. Ironless BLDCMs can overcome the above disadvantages and, owing to their high operating efficiency and low standby loss, are regarded as one of the best choices for FESS [173].

G. HOMOPOLAR MACHINE (HM)

The ACHM is categorized as a Homopolar Synchronous Machine (HSM) and Homopolar Inductor Alternator (HIA) [174], [175], [176]. The HM can offer advantages such as rigid rotor configuration, low idling losses, and high reliability, which make it significantly attractive for the high rotation velocity range [175], [176], [177], [178], [179], [180], [181]. Using the ACHM technology, the self-discharge will be lower; hence, the efficiency and energy density will be higher [180]. So, due to high efficiency, high rotation velocity range, and high energy density, ACHM is satisfactory to use in FESS [182], [183], [184]. Additionally, in the ACHM, the electromagnetic losses can be mitigated by disconnecting the excitation current when the FESS is idling, which aids the energy storage efficiency of the FESS, especially in long-term operating conditions [174]. The ACHM still suffers from disadvantages, including a unipolar air-gap flux density; thus, its power density is practically half of an electrical machine with a bipolar air-gap flux density [180]. In addition, all magnetic flux passing is axially through the rotor, so the air gap flux will be limited by the rotor diameter owing to the saturation of the iron core [185]. Since the rotor's angular velocity limits the rotor's diameter, the ACHM rotor's length and diameter are limited, limiting the machine's power and energy storage [125], [186]. An outer rotor ACHM with a FESS is suggested in [180] to have better energy storage capacity. Specifically, in [178], the electromagnetic function of a 30 KW ACHM is investigated and tested.

Accordingly, the summary of the above-investigated electrical machines' advantages and disadvantages is given in Table 5. Consequently, in the following section, these electrical machines will be investigated and analyzed comprehensively using the FEA by considering the FESS constraints.

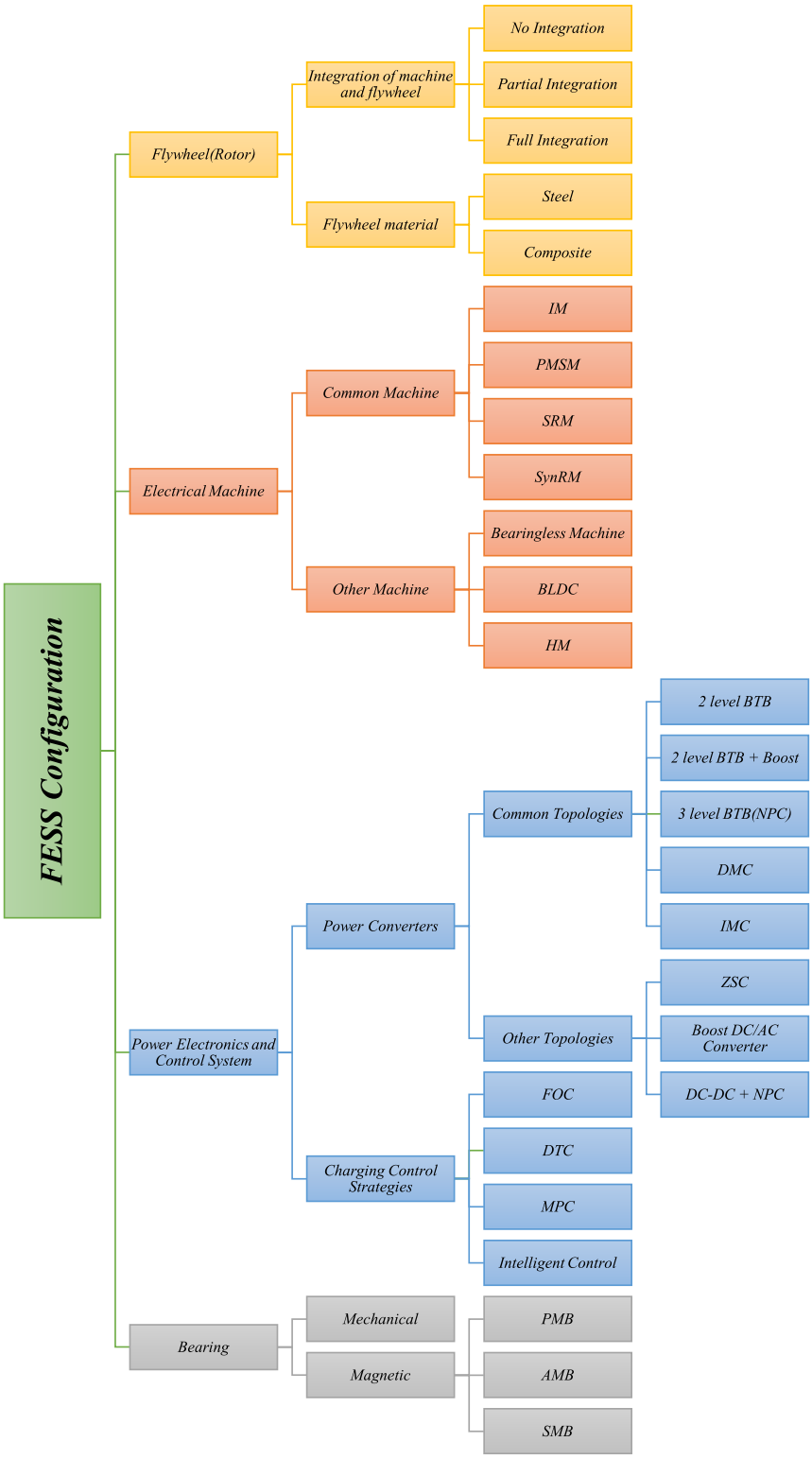

FIGURE 12. The main configuration of the FESS.

IV. COMPARATIVE STUDY OF THE SUPERIOR EMPLOYED MOTORS IN FESS

Based on the above review and Table 5, 1PMSM, SMPMSM, and SynRM have superiority over the other electrical machines to use in FESS, owing to their advantages over the other categories. Accordingly, in the following, the IPMSM, SMPMSM, and SynRM will be comprehensively investigated. Since the IM will not be satisfactory in HSFESS, and

TABLE 5. Summery of the investigated electrical machines' advantages and disadvantages.

Type of Machine	*Advantages*	*Disadvantages*
Induction Machine (IM)	• Rigid configuration • Low cost • High torque • High strength • High reliability	• Speed constraints, Control drive complexity • High-cost numerous maintenances • Lower efficiency than PMSM • High-speed challenges
Permanent Magnet Synchronous Machines (PMSM)	• High power density and efficiency • Higher power factor • Lower losses • Lower necessity for Volt-Ampere Inverters (VAIs)	• Subject to demagnetization due to having magnets • Have more sensitivity and vulnerability to warmth • The stator core's iron loss cause slows down it • Mechanical challenges in SMPMSM
Switched Reluctance Machine (SRM)	• Configuration simplicity and rigidness • Less iron loss • Ability to work in harsh environments and operating conditions • Simplicity in converter circuit design • Fault-tolerant ability	• High T_{ripple} • Vibration and Noise • Low Power Factor
Synchronous Reluctance Machine (SynRM)	• Satisfactory efficiency • High power capability • Configuration simplicity and rigidness • Wide speed range • Can be employed with PM	• High T_{ripple} • Vibration and Noise • Low Power Factor
Bearingless Machine	• Wide speed range • Long lifetime • No mechanical friction	• High cost and complexity
Brushless DC Machine (BLDC)	• High power density • High efficiency • Wide speed range • Mechanical stability • No EMI	• no-load losses are usually significant at high speeds • unbalanced forces during no-load
Homopolar Machine (HM)	• Rigid rotor configuration • Low idling losses • High reliability • Significantly attractive for high-speed range • High efficiency • High energy density	• Has a unipolar air-gap flux density, so its power density is practically half of an electrical machine with a bipolar air-gap flux density • All magnetic flux passing is axially through the rotor, so the air gap flux will be limited by the rotor diameter owing to saturation of the iron core • The HM rotor's length and diameter are limited, limiting the machine's power and energy storage

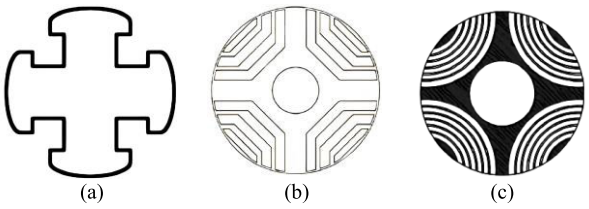

FIGURE 13. The types of SynRM rotor configurations, including (a) Single barrier rotor, (b) Axially laminated rotor, and (c) Transversally laminated rotor.

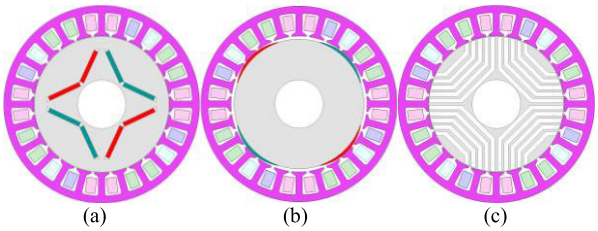

FIGURE 14. The topology of the investigated electrical machines, including (a) IPMSM, (b) SMPMSM, and (c) SynRM.

SRM has a very high T_{ripple}, which makes their usage in the FESS unsatisfactory, IM and SRM will not be regarded in the following investigations.

The topologies of the investigated electrical machines are shown in Fig. 14, which are analogous in Phase number, Pole number, air gap length of 0.48 mm, the materials in the laminations of stators and rotors, and the stators' configurations with the same outer and inner radius and the same number of slots. All the magnetic field analyses are the same in the stator current and the windings' fill factor. The stator

TABLE 6. The stator configurations' data of the investigated electrical machine models.

Designed Parameters	*Unit*	*Value*
Number of Phases	-	3
Number of Poles	-	4
Speed	RPM	10000
Line Peak Current	A	100
Current Density	A/mm^2	3.517
Parallel Paths	-	2
Stator Outer Diameter	mm	180
Stator Inner Diameter	mm	125
Type of Winding	-	Distributed
Stator Slots	-	24
Slot Depth	mm	21.1
Tooth Width	mm	6
Motor Length	mm	100
Material	-	M 19 24 Steel

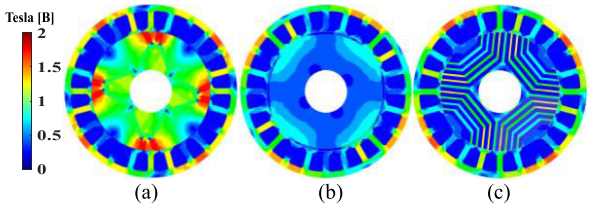

FIGURE 15. The flux density in the rotor and stator of (a) IPMSM, (b) SMPMSM, and (c) SynRM.

configurations' data of the investigated electrical machine models are given in Table 6.

A. COMPARING IPMSM, SMPMS, AND SynRM

1) FLUX DENSITY

The magnetic field density in the stator and rotor cores and the air-gap flux density are significant for the examination of the motors. The Permanent Magnet Synchronous Machines configurations are commonly categorized into IPMSM and SMPMSM. The same PM material (N30UH[1]) with B_r of 1125 mT is utilized in the above configurations' investigations [187]. The flux density of the above configurations is not analogous, owing to the dissimilarity in the magnet's arrangement and the leakage PM flux. Fig. 15 shows the flux density in the rotor and stator of IPMSM, SMPMSM, and SynRM. According to Fig. 16, which shows the load air-gap magnetic flux density of the above electrical machines, it can be seen that the stator current is more effective owing to the effective smaller air-gap in the IPMSM, besides the higher

[1]It belongs to the group of NdFeB magnets.

TABLE 7. Comparing the outcomes of FEA for IPMSM, SMPMSM, and, SynRM.

Parameters	*IPMSM*	*SMPMSM*	*SynRM*
Speed (RPM)	10000	10000	10000
Average Torque (Nm)	8.698	8.431	5.997
Torque Ripple (Nm)	1.233	1.077	0.999
Torque Ripple (%)	14.192	12.707	16.730
Power Factor	0.940	0.92	0.57
Output Power (W)	8380.5	8277.7	5493.4
Total Losses on Load (W)	825.1	705.930	872.090
System Efficiency (%)	91.037	92.142	86.3
Air Gap Flux Density (Average) (T)	0.239	0.263	0.233
Torque per Rotor Volume $(\frac{KNm}{m^3})$	7.186	7.011	4.942

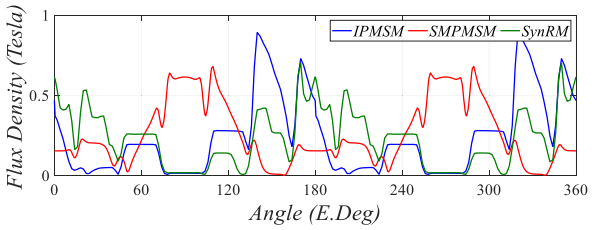

FIGURE 16. The load air-gap magnetic flux density of the studied electrical machines, including IPMSM, SMPMSM, and SynRM.

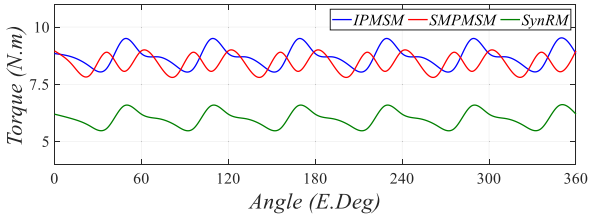

FIGURE 17. Torque distribution of the studied electrical machines, including IPMSM, SMPMSM, and SynRM.

maximum flux density in the air-gap than the SMPMSM. Moreover, in the SynRM, the maximum flux density in the air gap is higher than that of the SMPMSM and lower than the IPMSM. Increasing the flux density at the ribs of SynRM and PMSM is shown in Fig. 15, leading to the lower T_{ripple} [188]. According to Table 7, the average flux density in the air gap of the IPMSM is lower than the SMPMSM, which is due to the higher magnet leakage flux of the IPMSM.

2) TORQUE CHARACTERISTICS

According to Fig. 17 and Table 7, the Average Torque (T_{avg}) of the IPMSM is 3.07% and 31.06% higher than that of the SMPMSM and SynRM, respectively. Considering the

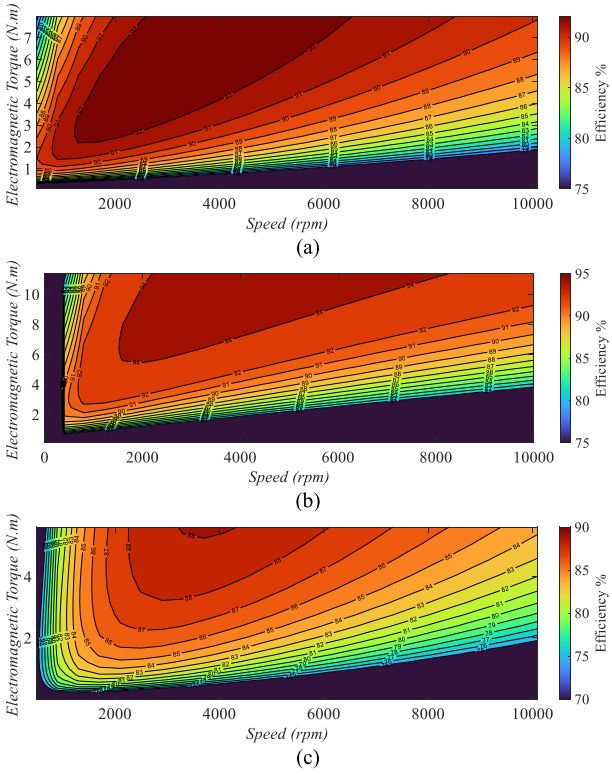

FIGURE 18. The efficiency maps under the MTPA control strategy, including (a) IPMSM, (b) SMPMSM, and (c) SynRM.

analogous constant angular velocity for operating conditions of IPMSM, SMPMSM, and SynRM give the same order of the output power (P_{out}) as that of the T_{avg}. The lowest and the highest T_{ripple} belong to the SMPMSM and the SynRM, respectively, since SMPMSM has no Reluctance Torque ($T_{reluctance}$) and SynRM has only $T_{reluctance}$.

3) EFFICIENCY AND POWER FACTOR

Determination of the stator and rotor iron losses (P_{core}) along with the magnet losses (P_{PM}) and copper winding losses (P_{cu}) gives total losses in load mode, as displayed in Table 7, and the efficiency of each motor is written as below:

$$\eta = \frac{P_{\text{out}}}{P_{\text{out}} + P_{\text{core}} + P_{\text{cu}} + P_{PM}} \tag{5}$$

According to Table 7, the efficiency and power factor of IPMSM and SMPMSM are practically the same. On the contrary, the SynRM has lower efficiency and power factor than the PMS motors.

Accordingly, the examinations endeavor to get a higher power factor in SynRM by optimizing the salience factor. Fig. 18 is the efficiency map under the Maximum Torque Per Ampere (MTPA) control strategy, displaying that the SMPMSM has the highest maximum efficiency.

4) FLUX-WEAKENING CAPABILITY

The optimal operation of the electric motor at a high rotation velocity range is one of the essential required features

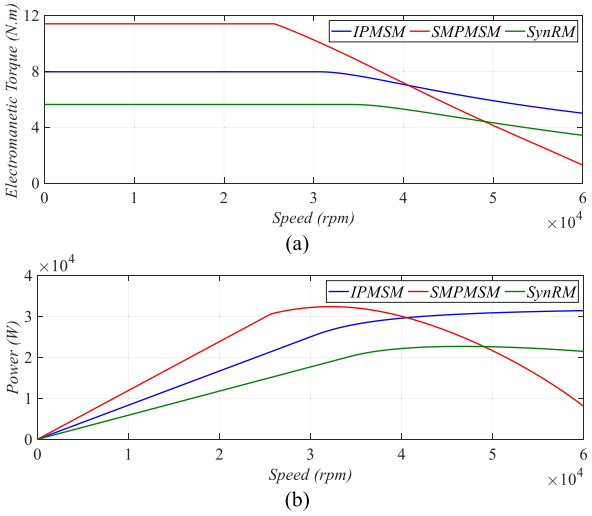

FIGURE 19. Comparing the T_{avg} and P_{out} at a wide speed range of the investigated electrical machines, including IPMSM, SMPMSM, and SynRM.

for FESS. Comparing the T_{em} and P_{out} at a wide rotation velocity range of the investigated motors is displayed in Fig. 19. Accordingly, the IPMSM gives more than 30 kW at 60,000 RPM, whereas SMPMSM has less than 10 kW and SynRM of about 22 kW. Thus, SMPMSMs are not satisfactory for FESS, requiring a Constant-Power Wide-Speed Range (CPWSR). Moreover, the SynRM is not inherently satisfactory to use in CPWSR, adding PMs in flux barriers will overcome this challenge [189].

Additionally, the SynRM has weaker magnetic characteristics, higher reliability, and easier maintenance than PMSM [190], [191], owing to the low heat in the winding and bearings and its simplicity, robustness, and lack of PM in rotor configuration. Besides the above merits, the manufacturing cost of a SynRM is much lower than PMS motors [192]. In hot areas and when the use of cooling systems is challenging, using the PMSMs has a high risk of demagnetization. The PMs in SMPMSMs should be fixed on the rotor surface against high centrifugal forces, which makes it unsatisfactory, especially in HSFESS. Consequently, in SMPMSMs, rotor sleeves are designed with high-strength alloys to overcome the above challenge, increasing the manufacturing cost of SMPMSM in HS-FESS. Accordingly, the SMPMSM is not satisfactory to use in HSFESS. Comparing the PMa-SynRM with the IPMSM is given in the following.

B. COMPARING PMa-SynRM AND IPMSM

According to the above analysis, the comparison of the PMa-SynRM with V-type IPMSM and SynRM is shown in the following. Due to the dissimilarity in operating conditions of PMa-SynRM in different PMs materials, two PMs materials, including ferrite and N30UH, have been regarded in this study. The topology of the designed PMa-SynRMs is displayed in Fig. 20.

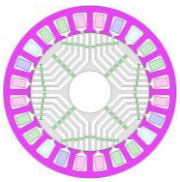

FIGURE 20. The topology of the investigated PMA-SynRM, including with ferrite and with N30UH material.

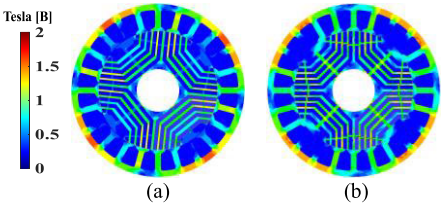

FIGURE 21. The on-load flux density in the rotor and stator of two types of PMA-SynRM, including (a) with ferrite and (b) with N30UH material.

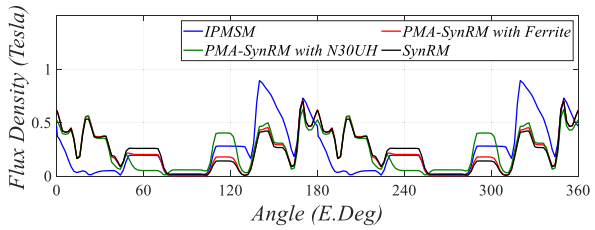

FIGURE 22. The on-load air-gap magnetic flux density of IPMSM, SynRM, and two types of PMA-SynRM with ferrite and N30UH PMs materials.

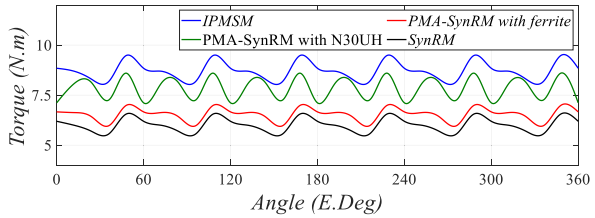

FIGURE 23. Torque diagram of the studied motors, including IPMSM, SynRM, and two types of PMA-SynRM with ferrite and N30UH PMs materials.

1) FLUX DENSITY

According to Fig. 21, which displays the on-load air-gap magnetic flux density of IPMSM, SynRM, and two types of PMa-SynRM with ferrite and N30UH PMs materials, owing to the more significant effective air-gap in the PMa-SynRM, it has a lower air-gap flux density than IPMSM with N30UH PM material. Moreover, the flux density in the air gap of the two types of PMa-SynRMs is analogous to the SynRM. Fig. 22 displays the on-load flux density in the rotor and stator of two types of PMa-SynRM. According to Table 8, the average flux density in the air gap of PMa-SynRM with N30UH is higher than that of SynRM.

2) TORQUE CHARACTERISTICS

Fig. 23 displays the torque diagram of the investigated motors, including IPMSM, SynRM, and two other types of PMa-SynRM with ferrite and N30UH PMs materials.

TABLE 8. Comparing the outcomes of FEA for IPMSM, SynRM, and two types of PMA-SynRM with ferrite and N30UH PMs materials.

Parameters	*IPMSM*	*SynRM*	*PMA-SynRM with Ferrite*	*PMA-SynRM with N30UH*
Speed (RPM)	10000	10000	10000	10000
Average Torque (Nm)	8.698	5.997	6.532	7.833
Torque Ripple (Nm)	1.233	0.999	1.019	1.503
Torque Ripple (%)	14.192	16.730	15.660	19.210
Power Factor	0.940	0.570	0.60	0.790
Output Power (W)	8380.5	5493.4	6052.8	7509.2
Total Losses on Load (W)	825.1	872.09	873.5	795.780
System Efficiency (%)	91.037	86.3	87.390	90.420
Air Gap Flux Density (Average) (T)	0.239	0.233	0.232	0.236
Torque per Rotor Volume $(\frac{KNm}{m^3})$	7.186	4.942	5.385	6.475

According to Fig. 23 and Table 8, increasing the T_{avg} and the torque density of both PMa-SynRMs is more significant than the SynRM configuration. Increasing the T_{avg} in the PMa-SynRM with PM N30UH and ferrite is 30% and 9%, respectively, more than T_{avg} of the SynRM, which is owing to the PM's torque term. Moreover, according to Table 8, adding PM makes the motor's torque density higher, which is more in the N30UH PM type than ferrite. By adding ferrite to the SynRM, T_{ripple} is better by 7%, and on the contrary, by adding N30UH, T_{ripple} is worse by 14%. Owing to that, the higher the magnetic flux between the rotor and the stator, the higher the T_{ripple}. Consequently, when the rare earth magnet is utilized in the SynRM, the magnetic flux will grow, and the T_{ripple} will be higher. In general, by adding PM to the SynRM, the T_{avg} of PMa-SynRM will be analogous to IPMSM.

3) EFFICIENCY AND POWER FACTOR

According to Table 8, increasing the efficiency of both PMa-SynRMs can be seen by 4.7% and 1.3% in PMa-SynRM with N30UH and ferrite more than SynRM efficiency, respectively. Moreover, increasing the power factor of PMa-SynRM with N30UH and ferrite is 37.4% and 7.1% more than SynRM, respectively. In Fig. 24, the efficiency maps under the MTPA control strategy are displayed, in which the

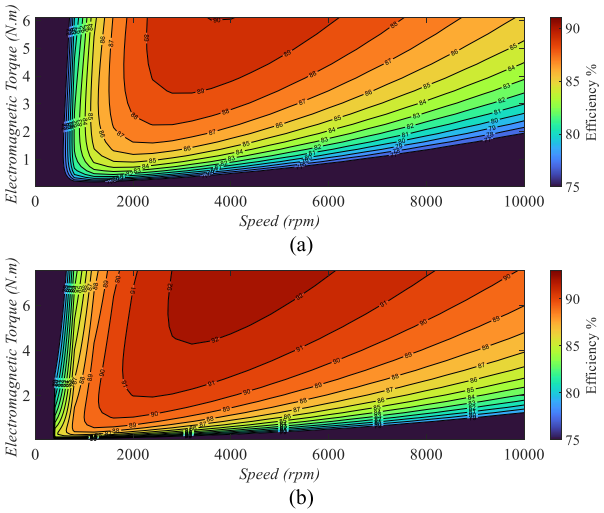

FIGURE 24. The efficiency maps under the MTPA control strategy of two types of PMA-SynRM, including (a) with ferrite and (b) with N30UH material.

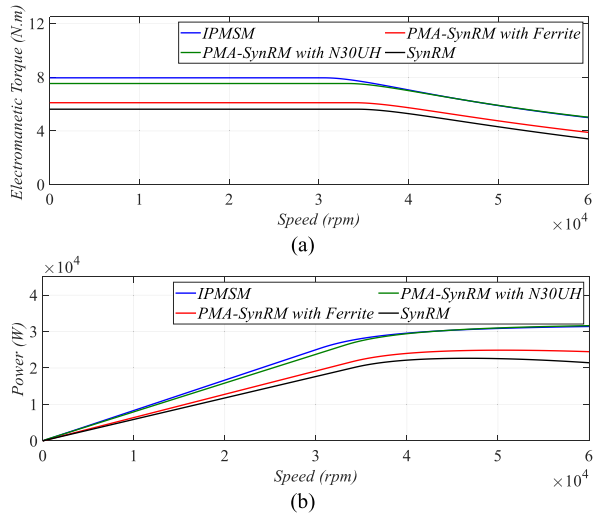

FIGURE 25. Comparing the T_{avg} and P_{out} at a wide speed range of two types of PMA-SynRM, including (a) with ferrite and (b) with N30UH.

PMa-SynRM with N30UH has the highest maximum efficiency.

4) HIGH-SPEED FLUX-WEAKENING CAPABILITY

Comparing the T_{em} and P_{out} of the investigated motors in Fig. 25, including IPMSM, SynRM, and two types of PMa-SynRM with ferrite and N30UH PMs materials, shows that, at high rotation velocity range, both PMa-SynRMs have a better operating point than that of the SynRM. Accordingly, the PMa-SynRM with N30UH PMs materials gives an analogous P_{out} with IPMSM at 60000 RPM. Whereas PMa-SynRM with ferrite has less P_{out} than PMa-SynRM with N30UH and more P_{out} than SynRM. Thus, adding PM to SynRM as PMa-SynRM gives a better operating point in CPWSR than SynRM. Also, the higher value of the

TABLE 9. The cost of employed materials in investigated PM motors, including PMA-SynRM with ferrite, PMA-SynRM N30UH, and IPMSM.

Parameters	*IPMSM*	*PMA-SynRM with Ferrite*	*PMA-SynRM with N30UH*
Stator Lam Weight (kg)	5.310	5.310	5.310
Armature Copper Weight (kg)	3.970	3.970	3.970
Slot Wedge Weight (kg)	0.036	0.036	0.036
Rotor Lam Weight (kg)	7.186	3.512	3.512
Magnet Weight (kg)	0.708	0.268	0.418
Total Costs (USD)	137.659	43.838	95.721

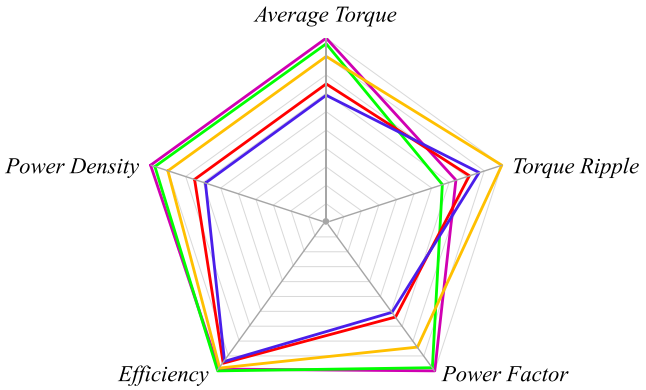

FIGURE 26. Comparing the effective indexes in the FESS between the studied motors in terms of Per Unit (P.U), including IPMSM (Purple), SMPMSM (Green), PMA-SynRM with Ferrite (Red), PMA-SynRM with N30UH (Yellow), SynRM (Blue).

$(B \times H)_{Max}$ for the used PM in PMa-SynRM gives a better P_{out} and T_{em} in HSFESS.

5) COST

Cost is one of the most significant factors in choosing an electrical machine to use in FESS. Therefore, the cost of the used materials in the investigated PM motors, including PMa-SynRM with ferrite, PMa-SynRM N30UH, and IPMSM, is given in Table 9. The unit costs for iron lamination, copper, ferrite, and N30UH magnet are regarded to be 1.45 $\$/kg$ [193], 7.5915 $\$/kg$ [194], 3.2 $\$/kg$ [195], and 126.2 $\$/kg$ [195], respectively. Accordingly, the lowest cost is for PMa-SynRM with ferrite, followed by PMa-SynRM with N30UH, and the highest one is for the IPMSM configuration. Generally, according to Fig. 26, PMa-SynRM is better than SynRM and is satisfactorily close to IPMSM. On the hand of economic concerns, SynRM can be a satisfactory item. But based on electrical characteristics,

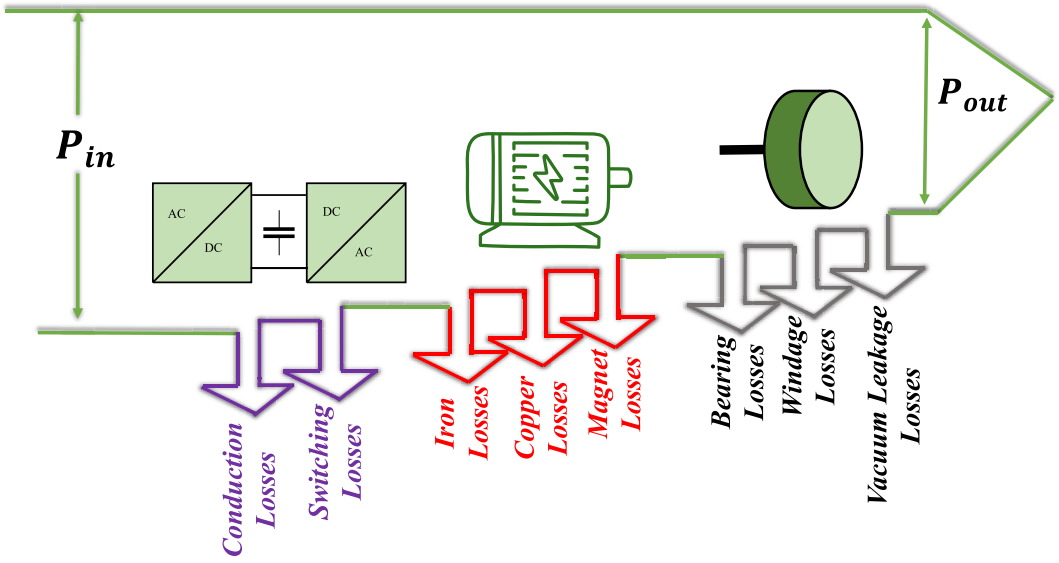

FIGURE 27. A summary overview of efficiency calculation and different losses in the flywheel system.

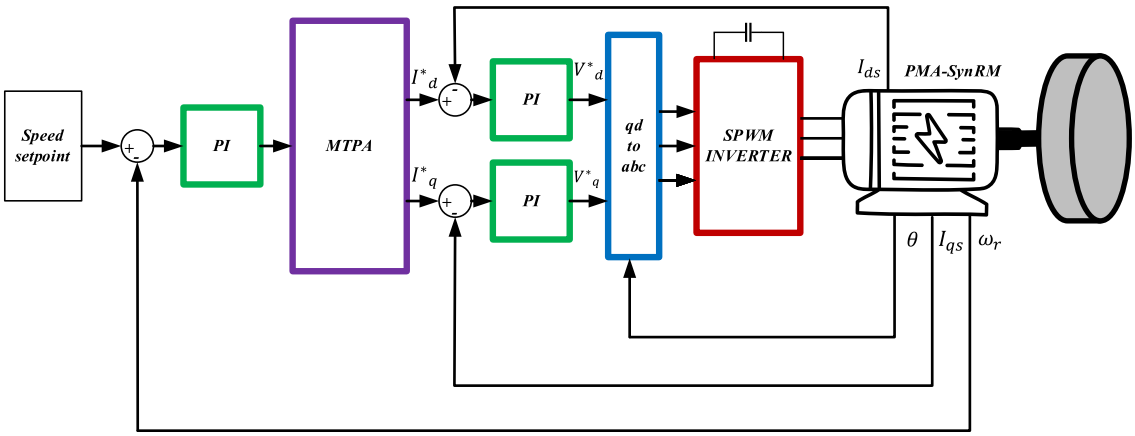

FIGURE 28. Accurate digital controller, which is systematically designed by the Field Oriented Control algorithm [72].

IPMSM is more satisfactory. Owing to the lower cost and the higher reliability of the PMa-SynRM, it will have a high superiority over the other rivals, if both metrics are regarded.

Given that energy efficiency has a direct and indirect effect on the operating condition of the system and its cost, respectively, it is one of the key metrics for the assessment of an energy storage system [38]. So, high efficiency can be regarded as an attribute of usable capacity, since the former leads to the latter. Accordingly, the main losses that must be regarded in the FESS are bearings' friction losses, wind losses around the rotating elements (rotor and flywheel), windings losses, iron losses in the electric machine (stator and rotor), vacuum leakage losses, serration losses due to magnetic float and losses in power electronics converter [38]. In Fig. 27, a summary overview of efficiency calculation and different losses in the flywheel system is displayed.

V. THE LABORATORY PROGRESS IN THE FIELD OF FESS

Our laboratory investigation and progress in the field of FESS such as introducing robust control strategies [72], [87] and the new design of PMa-SynRM [197] are reviewed in the following section, which can be regarded as a guide for the engineering community.

A. IMPLEMENTING AND DESIGNING OF A CONTROL SYSTEM WITH THE ABILITY TO WITHSTAND MEASUREMENT ERROR FOR THE FESS [72]

Proposing a control system for the FESS with PMa-SynRM, which can withstand measurement error is a big honor. The PMa-SynRM inherently has a T_{ripple}. Moreover, the lack of satisfactory design and switching algorithms can cause more mechanical damage.

Accordingly, in [72] an accurate digital controller is systematically designed by the FOC algorithm, as shown in

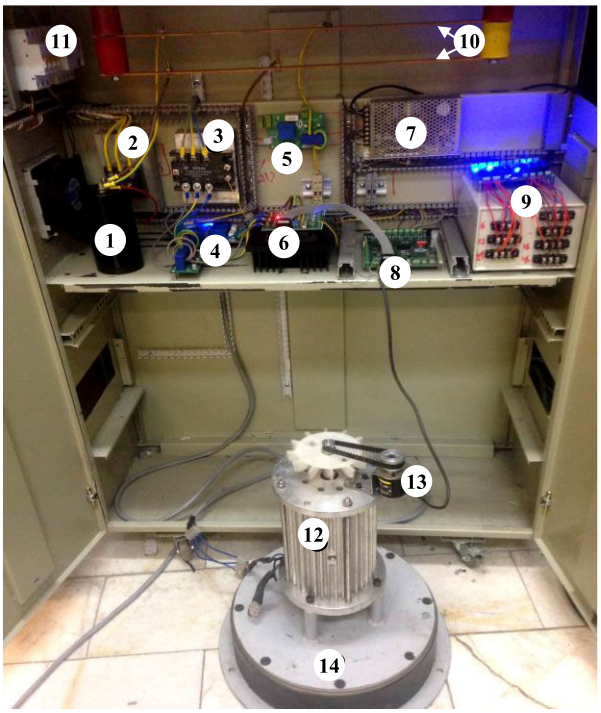

FIGURE 29. FESS Test bench, including 1-DC-Link Capacitor, 2-Three-Phase Diode Rectifier, 3- Solid State Relay (SSR), 4- AC Current and Voltage Sensor, 5- DC Current and Voltage Sensor, 6- IPM 3-Phase Inverter, 7- Switching Power Supply, 8- DSP Control Board, 9- Isolated Power Supply, 10- DC-Link, 11- Protection Fuses, 12- PMA-SynRM, 13-Encoder, 14- Flywheel Disk [72].

Fig. 28. For improving the PMa-SynRM control in the transient states, The MTPA can be employed as a kind of FOC strategy. It was shown that if no error is in the measurement, enhancing the motor's acceleration and remaining within the nominal operating range of T_{em} will be obtained, through the designed controllers. Thus, it can be argued that the designed controller can be employed optimally in the FESS for continuous charging and discharging in this system. The test bench is displayed in Fig. 29. According to outcomes in [72], it can be seen that although the control system is designed precisely, measurement error significantly affects the system. The dead zone and measurement offset inject the non-ideality in the current individually, leading to the oscillation of rotor velocity. In the worst case, if the offset and dead zone are in the current sensor simultaneously, the motor stability will fail. Hence, the function of the designed controller relies on the accuracy of the analog measurement. Accordingly, the design and use of High Pass Frequency (HPF) and Finite Impulse Response (FIR) filters appropriately in the designed control system can overcome the offset and dead zone challenges. Details of the employed filters are given in Table 10. Moreover, by implementing the designed filters in the drive system, the offset and dead zone errors are mitigated, and it gives lower rotor velocity oscillations. The suggested filters have advantages, such as accessibility and simplicity in design and usage. In Table 11, comparing the suggested strategy with

TABLE 10. Details of the employed filters, including HPF and FIR [72].

HPF		*FIR*	
Characteristics	*Frequency*	*Characteristics*	*Frequency*
Cut-off Frequency	0.1 Hz	Passband Edge Frequency	100 Hz
		Stopband Edge Frequency	120 Hz
		Maximum Passband Ripple	0.1 dB
Sample Frequency	4 kHz	Minimum Stopband Attenuation	120 dB
		Input Sample Rate	4 kHz
		Filter order N	2

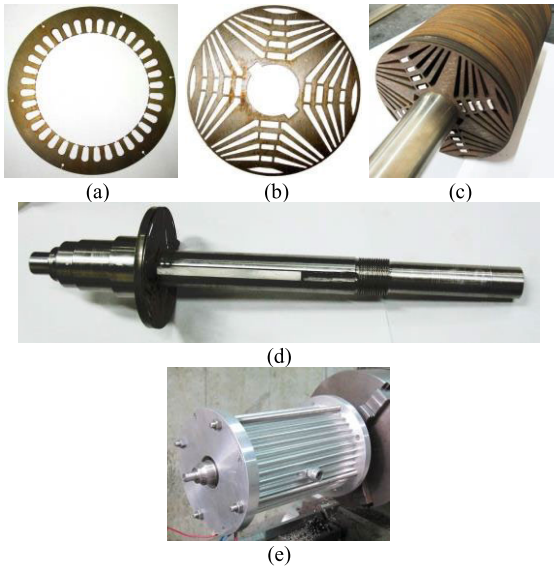

FIGURE 30. Prototype configuration of PMA-SynRM, including (a) Wirecut of stator, (b) Wirecut of rotor, (c) Placing PMs in barriers, (d) Rotor shaft, and (e) Aluminium frame.

others is displayed. Technical data of PMa-SynRM and its prototype configuration separately are given and displayed in Table 12 and Fig. 30, respectively.

In order to verify the suggested controller, with 2.4 kW PMa-SynRM and using the DSP TMS320F28335, the measurement results are experimentally investigated. An Omron Encoder E6B2-CWZ6C with a resolution of 2000 is the rotor angle and angular velocity sensor. Moreover, the test bench is shown in Fig. 29. Accordingly, the measurement of the angular velocity and stator currents are shown in Fig. 31. According to Fig. 31(a), the magnitude of the stator current at the first start is high to reach the base angular velocity.

TABLE 11. Comparing the suggested strategy with others [72].

Method	*Implementation*	*Cost*	*Computational Time*	*Offset & Dead Zone Elimination*	*Phase and Amplitude Errors*
Proposed HPF+FIR	Simple	Low	Low	Both	No
Network based detector	Complex	Medium	High	Offset	No
Second order band-pass filter (BPF)+low-pass filter (LPF)	Simple	Low	Low	Offset	Yes
One algorithm by using of the integrator output signal d-axis proportional plus integral (PI) current regulator.	Complex	Low	High	Offset	No
Multi-sensor switching strategy and associated observers that estimate the rotor flux	Complex	High	High	Offset	No
Notch filter	Simple	Low	Low	Both	Yes

TABLE 12. Technical data of PMA-SynRM.

Parameter	*Unit*	*Value*	*Parameter*	*Unit*	*Value*
Stator d axes inductances (L_{ds})	*mH*	55	Rated Power	*KW*	2.4
Stator q axes inductances (L_{qs})	*mH*	23	Rated Speed	*rpm*	600
Rotor inertia (J)	$kg.m^2$	0.04	Phase voltage	*V*	380
Stator single-phase resistance (r_s)	Ω	3.5	Phase current	*A*	9
Number of motor poles (P)	-	4	Power factor	-	0.78
Magnet flux added to the rotor (λ)	*Wb*	0.1			
Air friction coefficient of flywheel disk (K_f)	-	0.0001			

TABLE 13. Comparing the designed MPC and PI controller [87].

Controller Type	*Motor current THD (%)*	*Time From 6000–3000 RPM*	*Time from 6000-5800 RPM*	*Speed Variation in 15% Load Increase*	*Steady State Ripple*	*Starting Torque Ripple*
MPC	7.4	3.15 *S*	0.03 *S*	- 7 *RPM*	0.02 *N.m*	0.4 *N.m*
PI	9.38	3.15 S	0.10 *S*	- 15 *RPM*	0.052 *N.m*	0.6 *N.m*

TABLE 14. Comparing between IPM-SynRM and PMA-SynRM [197].

Characteristic	*PMA-SynRM*	*IPM-SynRM*
Average torque (N.m)	9.90	11.44
Torque Ripple (%)	52.4	16.0
PM Volume (cm^3)	19.6	13.92
Power Factor (%)	76.3	82.1
Efficiency (%)	89.2	90.1
Copper loss (W)	139.3	139.3
Iron loss (W)	49.5	57.9

Then, the stator current will lower. Additionally, as shown in Fig. 31(b), the motor's acceleration rate is satisfactory and reaches its steady value with a negligible steady-state error. Given that the T_{em} of the motor is 3.9 Nm, the reference

TABLE 15. Summery of the our laboratory investigations in FESS.

	Novelty	*Problems*	*Soloution*	*Features*
Control Drive System	[72]	The measurement errors such as offset and dead zone will cause increasing of angular velocity and system instability	Employing of HPF and FIR filters	Remove the offset and dead zone errors and fix the angular velocity oscillations and instability The suggested filters have advantages, including no phase and amplitude errors, accessibility in design, simplicity in employ and relatively low sensitivity to quantifying
	[87]	The non-linear dynamics and dependency on operating points in-time compensating power is necessary in FESS	Suggesting a linear dynamic for PMA-SynRM and employing CCS-MPC algorithm	Lower T_{ripple}, faster and more accurate dynamic, solves the complexity of designing non-linear methods and the dependency on operating points, more ACC rate
Electrical Machine Configuration	[197]	Conventional rotor configuration in PMA-SynRM brings constraint to T_{avg}	Suggesting a new type as IPM-SynRM	Increasing T_{avg} by 15% while 29% less employed PM, reducing T_{ripple} by 70%, improving PM flux linkage per unit PM mass up to 340%, and increasing the load level, power factor, and efficiency

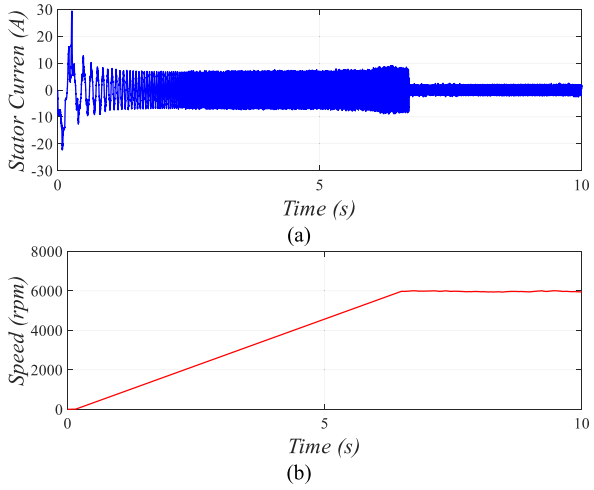

FIGURE 31. Measurement of PMa-SynRM experimentally, including (a) stator curren and (b) rotation velocity [72].

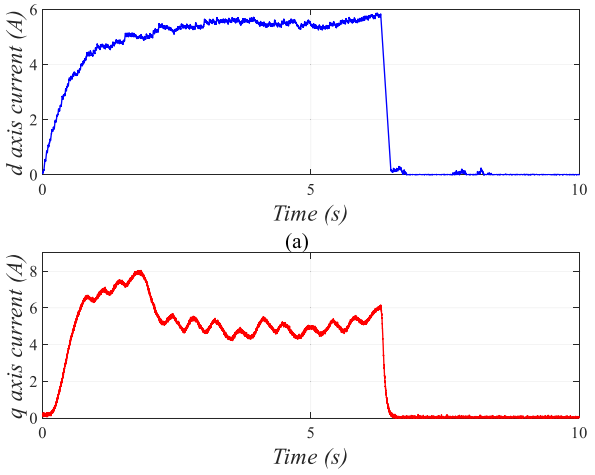

FIGURE 32. Measurement of I_{dq} for PMa-SynRM experimentally [72].

acceleration rate is written as $\frac{T_e}{j} = \frac{d\omega_r}{dt}$, which must be about 95 rad/s^2. Fig. 32 shows the measurement of I_{dq}. After reaching the rotor angular velocity to the base rate, I_{dq} lower to near zero.

B. THE CONTINUOUS CONTROL SET (CCS)-MPC FOR THE PERMANENT MAGNET-ASSISTED SYNCHRONOUS RELUCTANCE MOTOR (PMa-SynRM) IN FESS [87]

Owing to the non-zero current in the d-axis, the non-linear dynamic is the main challenge of the PMa-SynRM drive system. Accordingly, in [87], a linear dynamic for the PMa-SynRM is suggested, which solves the complexity of designing non-linear methods. So, the augmented linear model can be employed to design an MPC for the PMa-SynRM drive system [87].

MPC has simplicity in design and can be used in Multiple Input/Multiple Output systems (MIMO), such as Continuous Control Set (CCS)-MPC and Finite Control Set (FCS)-MPC. In CCS-MPC, according to the system's dynamic, the control signals are generated. On the other hand, in the FCS-MPC, a switching mode is chosen among the number of switching states. Moreover, a modulator gives a fixed switching frequency, to generate control signals in CCS-MPC. It should be noted that using CCS-MPC leads to less T_{ripple} and lower steady-state error in SRMs. The designed CCS-MPC algorithm to control PMa-SynRM, using an augmented linearized model, is shown in Fig. 33.

Using an MPC will give faster and more accurate dynamics, more acceleration rate, fewer oscillations, more effective torque, less angular velocity dropping, and less recovery time and steady-state error than the Proportional-Integral (PI)

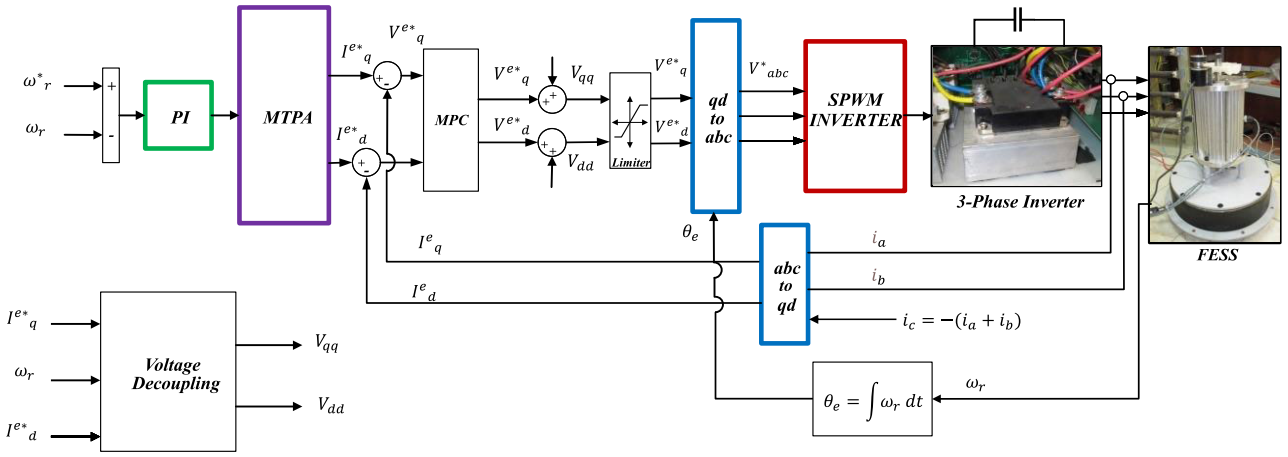

FIGURE 33. The designed CCS-MPC algorithm for PMA-SynRM drive control [87].

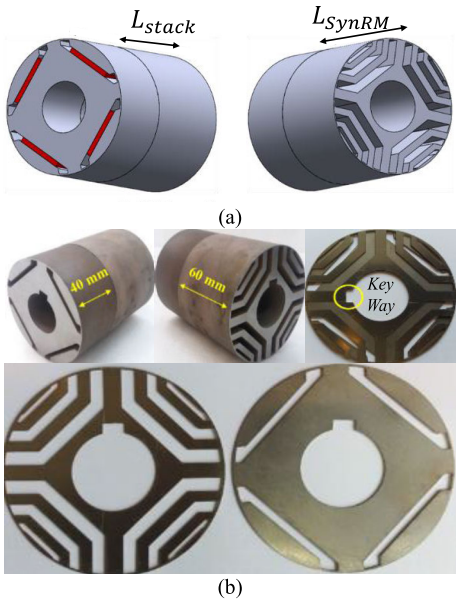

FIGURE 34. The suggested IPM-SynRM, (a) 3D view of rotor configuration, (b) Prototype configuration: Laminations and assembeling [197].

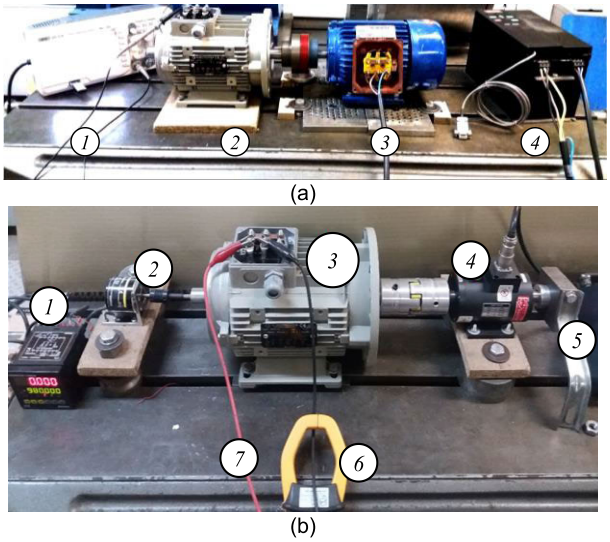

FIGURE 35. Provided test bench, (a) no load, including 1-Oscilloscope 2-Prototype 3-Prime motor 4-Inverter and (b) static load, including 1-Counter 2-Encoder 3-Test Motor 4-Torque Sensor 5- Rotor Locking Tool 6- CT 7-DC Current [197].

controllers, which makes the MPC more eligible for FESS. In [87], the effectiveness and fast dynamics of the designed PMa-SynRM control strategy for FESS are displayed experimentally against the PI controller and FCS-MPC. Comparing the designed MPC and PI controller is shown in Table 13.

C. DESIGN OF MODIFIED PMa-SynRM FOR IMPROVING ITS TORQUE AND EFFICIENCY IN FESS [197]

The design of IPM-SynRM, which is satisfactory for FESS owing to its advantages, is the other progress in the field of FESS. Since placing of PM materials is usually into the flux barriers region of the rotor and PMs' size relies on the available area of the barriers, using the PMs' advantages is not efficient. The PMa-SynRM rotor consists of two segments, including the Interior PM (IPM) and the SynRM. In IPM-SynRM the above segments are installed axially on the shaft. Fig. 34 shows the Three-Dimensional (3D) views of the built IPM-SynRM rotor. According to [197], increasing the T_{em} by 15% and decreasing the T_{ripple} by 70% is the merits of the designed IPM-SynRM.

Contrary to the SynRMs and PMa-SynRMs, the T_{ripple} rate of IPM-SynRM will be lower with increasing load level. Moreover, PM flux linkage is significantly more in IPM-SynRM, which is owing to the design of PMs (i.e., sizes and how arrangement) not relying on the SynRM design. So, increasing PM flux linkage per unit PM mass by up to 340% is yielded. The built prototype of the designed IPM-SynRM along with the test bench is shown in Fig. 35. Comparing the power factor, T_{avg}, T_{ripple}, PM volume, electromagnetic losses, and efficiency between IPM-SynRM and

PMa-SynRM are displayed in Table 14. Accordingly, IPM-SynRM has more efficiency, higher T_{avg}, higher P_{out}, higher power factor, and lower losses than PMa-SynRM, showing the superiority of IPM-SynRM usage.

Accordingly, in the above section, the laboratory progress in the field of FESS, such as robust control algorithms of PMa-SynRM and IPM-SynRM design were reviewed, which give advantages, especially in the FESS usages, as displayed in Table 15.

VI. CONCLUSION

The FESS has lots of benefits, including long lifetime, few contaminations, fast dynamic, and high charging/discharging capability. The FESS can be used in EVs, railways, and renewable energy systems. The total charges and discharge cycles of FESS are very high, and it can transfer high energy in a short time (seconds to minutes). Accordingly, FESS has superiority in sustainability, especially for high-cycle and high-power storage systems. Since the efficiency, power rating, cost, angular velocity, power factor, weight, and volume of FESS have a high dependency on the electrical machine, power electronics converter, and control system, which have the most significant role in transferring energy, this study comprehensively reviews them according to FESS usage.

Accordingly, the FESS's configurations, including flywheel (rotor), electrical machines (motor/generator), power electronics converters, control systems, and bearings, are investigated in detail. So, the review of electrical machines' control systems and bidirectional converters displayed that the most concentrations are on the FOC strategy in PMSMs and IMs and the two-level BTB converters. On the other hand, using PMa-SynRM, and especially the suggested IPM-SynRM, can be regarded as a satisfactory suggestion to use in the FESS.

The FESS has two main categories, in terms of rotation velocity, including HSFESS and LSFESS. Composite flywheel (rotor) and magnetic bearings are employed in HSFESS. In LSFESS, a steel flywheel and mechanical or mixed (mechanical and magnetic) bearings are employed. Since HSFESSs have more usage, electrical machines with the capability of high rotation velocity should be regarded, such as PMSM, SynRM, and PMa-SynRM.

Conventional electrical machines in FESS are IM, PMSM, SRM, and SynRM. SRM has a high T_{ripple}, and IM is not satisfactory for HSFESS. PMSM has the advantages of high power density, high efficiency, and high power factor, though the iron loss causes constraints on it. SynRM has advantages such as low-cost manufacturing, high efficiency, and high mechanical strength, whereas it has challenges such as low power factor, low torque density, and large T_{ripple}. Since the electrical machines' T_{avg}, T_{ripple}, and power factor have significant effects on FESS, the PMa-SynRM machine is suggested and investigated. PMa-SynRM gives better power factor and torque density, owing to T_{PM} besides $T_{reluctance}$, which has the advantages of PMSM and SynRM, simultaneously. In addition, PMa-SynRM has the advantages of rotor configuration simplicity, control simplicity, and less power loss owing to the lack of rotor current.

Finally, the outcomes of the laboratory in FESS, including the design of electrical machines and their control algorithms, are investigated in the above review study. Since the measurement errors will cause higher angular velocity and system instability, using HPF and FIR filters will remove the offset and dead zone errors and fix the angular velocity oscillations in FESS. Additionally, using the suggested CCS-MPC gives a faster and more accurate dynamic and less T_{ripple}. On the other hand, the IPM-SynRM is a new configuration of PMa-SynRM, which has advantages such as increasing T_{avg} by 15% while 29% less used PM, reducing T_{ripple} by 70%, improving PM flux linkage per unit PM mass up to 340%, and increasing the load level, power factor, and efficiency.

REFERENCES

[1] X. Li and A. Palazzolo, "A review of flywheel energy storage systems: State of the art and opportunities," *J. Energy Storage*, vol. 46, Feb. 2022, Art. no. 103576, doi: 10.1016/j.est.2021.103576.

[2] F. Zhang, P. Zhao, M. Niu, and J. Maddy, "The survey of key technologies in hydrogen energy storage," *Int. J. Hydrogen Energy*, vol. 41, no. 33, pp. 14535–14552, Sep. 2016, doi: 10.1016/j.ijhydene.2016.05.293.

[3] M. A. Hannan, S. B. Wali, P. J. Ker, M. S. A. Rahman, M. Mansor, V. K. Ramachandaramurthy, K. M. Muttaqi, T. M. I. Mahlia, and Z. Y. Dong, "Battery energy-storage system: A review of technologies, optimization objectives, constraints, approaches, and outstanding issues," *J. Energy Storage*, vol. 42, Oct. 2021, Art. no. 103023, doi: 10.1016/j.est.2021.103023.

[4] H. Ibrahim, K. Belmokhtar, and M. Ghandour, "Investigation of usage of compressed air energy storage for power generation system improving—Application in a microgrid integrating wind energy," *Energy Proc.*, vol. 73, pp. 305–316, Jun. 2015, doi: 10.1016/j.egypro.2015.07.694.

[5] H. Yang, "A review of supercapacitor-based energy storage systems for microgrid applications," in *Proc. IEEE Power Energy Soc. Gen. Meeting (PESGM)*, Aug. 2018, pp. 1–5, doi: 10.1109/PESGM.2018.8585956.

[6] G. Li, "Energy and exergy performance assessments for latent heat thermal energy storage systems," *Renew. Sustain. Energy Rev.*, vol. 51, pp. 926–954, Nov. 2015, doi: 10.1016/j.rser.2015.06.052.

[7] S. Rehman, L. M. Al-Hadhrami, and M. M. Alam, "Pumped hydro energy storage system: A technological review," *Renew. Sustain. Energy Rev.*, vol. 44, pp. 586–598, Apr. 2015, doi: 10.1016/j.rser.2014.12.040.

[8] A. Berrada, K. Loudiyi, and I. Zorkani, "System design and economic performance of gravity energy storage," *J. Cleaner Prod.*, vol. 156, pp. 317–326, Jul. 2017, doi: 10.1016/j.jclepro.2017.04.043.

[9] Z. Zhang, T. Ding, Q. Zhou, Y. Sun, M. Qu, Z. Zeng, Y. Ju, L. Li, K. Wang, and F. Chi, "A review of technologies and applications on versatile energy storage systems," *Renew. Sustain. Energy Rev.*, vol. 148, Sep. 2021, Art. no. 111263, doi: 10.1016/j.rser.2021.111263.

[10] B. Zakeri and S. Syri, "Electrical energy storage systems: A comparative life cycle cost analysis," *Renew. Sustain. Energy Rev.*, vol. 42, pp. 569–596, Feb. 2015, doi: 10.1016/j.rser.2014.10.011.

[11] D. Schulz, "Grid integration of wind energy systems," in *Power Electronics in Smart Electrical Energy Networks* (Power Systems), vol. 34. London, U.K.: Springer, 2008, pp. 327–374, doi: 10.1007/978-1-84800-318-7_11.

[12] D. Y. Goswami and F. Kreith, *Energy Conversion*, 2nd ed. Boca Raton, FL, USA: CRC Press, 2017, doi: 10.1201/9781315374192.

[13] H. Chen, T. N. Cong, W. Yang, C. Tan, Y. Li, and Y. Ding, "Progress in electrical energy storage system: A critical review," *Prog. Natural Sci.*, vol. 19, no. 3, pp. 291–312, Mar. 2009, doi: 10.1016/j.pnsc.2008.07.014.

[14] K. R. Pullen, "Flywheel energy storage," in *Storing Energy*. Amsterdam, The Netherlands: Elsevier, 2022, pp. 207–242, doi: 10.1016/B978-0-12-824510-1.00035-0.

[15] S. Vazquez, S. M. Lukic, E. Galvan, L. G. Franquelo, and J. M. Carrasco, "Energy storage systems for transport and grid applications," *IEEE Trans. Ind. Electron.*, vol. 57, no. 12, pp. 3881–3895, Dec. 2010, doi: 10.1109/TIE.2010.2076414.

[16] G. Ren, G. Ma, and N. Cong, "Review of electrical energy storage system for vehicular applications," *Renew. Sustain. Energy Rev.*, vol. 41, pp. 225–236, Jan. 2015, doi: 10.1016/j.rser.2014.08.003.
[17] G. J. Hoolboom and B. Szabados, "Nonpolluting automobiles," *IEEE Trans. Veh. Technol.*, vol. 43, no. 4, pp. 1136–1144, Nov. 1994, doi: 10.1109/25.330178.
[18] X. Zhou and J. Fang, "Precise braking torque control for attitude control flywheel with small inductance brushless DC motor," *IEEE Trans. Power Electron.*, vol. 28, no. 11, pp. 5380–5390, Nov. 2013, doi: 10.1109/TPEL.2013.2244617.
[19] A. Rupp, H. Baier, P. Mertiny, and M. Secanell, "Analysis of a flywheel energy storage system for light rail transit," *Energy*, vol. 107, pp. 625–638, Jul. 2016, doi: 10.1016/j.energy.2016.04.051.
[20] T. Ratniyomchai, S. Hillmansen, and P. Tricoli, "Recent developments and applications of energy storage devices in electrified railways," *IET Electr. Syst. Transp.*, vol. 4, no. 1, pp. 9–20, Mar. 2014, doi: 10.1049/iet-est.2013.0031.
[21] H. Lee, S. Jung, Y. Cho, D. Yoon, and G. Jang, "Peak power reduction and energy efficiency improvement with the superconducting flywheel energy storage in electric railway system," *Phys. C, Supercond. Appl.*, vol. 494, pp. 246–249, Nov. 2013, doi: 10.1016/j.physc.2013.04.033.
[22] G. O. Cimuca, C. Saudemont, B. Robyns, and M. M. Radulescu, "Control and performance evaluation of a flywheel energy-storage system associated to a variable-speed wind generator," *IEEE Trans. Ind. Electron.*, vol. 53, no. 4, pp. 1074–1085, Jun. 2006, doi: 10.1109/TIE.2006.878326.
[23] R. Cárdenas, R. Peña, G. Asher, and J. Clare, "Power smoothing in wind generation systems using a sensorless vector controlled induction machine driving a flywheel," *IEEE Trans. Energy Convers.*, vol. 19, no. 1, pp. 206–216, Mar. 2004, doi: 10.1109/TEC.2003.816605.
[24] R. Cárdenas, R. Peña, G. M. Asher, J. Clare, and R. Blasco-Gimenez, "Control strategies for power smoothing using a flywheel driven by a sensorless vector-controlled induction machine operating in a wide speed range," *IEEE Trans. Ind. Electron.*, vol. 51, no. 3, pp. 603–614, Jun. 2004, doi: 10.1109/TIE.2004.825345.
[25] M. Ghanaatian and S. Lotfifard, "Control of flywheel energy storage systems in the presence of uncertainties," *IEEE Trans. Sustain. Energy*, vol. 10, no. 1, pp. 36–45, Jan. 2019, doi: 10.1109/TSTE.2018.2822281.
[26] G. Cimuca, S. Breban, M. M. Radulescu, C. Saudemont, and B. Robyns, "Design and control strategies of an induction-machine-based flywheel energy storage system associated to a variable-speed wind generator," *IEEE Trans. Energy Convers.*, vol. 25, no. 2, pp. 526–534, Jun. 2010, doi: 10.1109/TEC.2010.2045925.
[27] M. Melissa. (2004). *Flywheel Energy Storage System*. Accessed: Aug. 10, 2022. [Online]. Available: http://www.123seminarsonly.com/Seminar-Reports/020/35222269-Flywheel-Energy-Storage-System.pdf
[28] A. Saleh, A. Awad, and W. Ghanem, "Modeling, control, and simulation of a new topology of flywheel energy storage systems in microgrids," *IEEE Access*, vol. 7, pp. 160363–160376, 2019, doi: 10.1109/ACCESS.2019.2951029.
[29] B. Zhao, X. Zhang, and J. Chen, "Integrated microgrid laboratory system," *IEEE Trans. Power Syst.*, vol. 27, no. 4, pp. 2175–2185, Nov. 2012, doi: 10.1109/TPWRS.2012.2192140.
[30] M. L. Lazarewicz and A. Rojas, "Grid frequency regulation by recycling electrical energy in flywheels," in *Proc. IEEE Power Eng. Soc. Gen. Meeting*, vol. 2, Jun. 2004, pp. 2038–2042, doi: 10.1109/PES.2004.1373235.
[31] L. Zhou and Z. P. Qi, "Modeling and control of a flywheel energy storage system for uninterruptible power supply," in *Proc. Int. Conf. Sustain. Power Gener. Supply*, Apr. 2009, pp. 1–6, doi: 10.1109/SUPERGEN.2009.5348077.
[32] Y. Suzuki, A. Koyanagi, M. Kobayashi, and R. Shimada, "Novel applications of the flywheel energy storage system," *Energy*, vol. 30, nos. 11–12, pp. 2128–2143, Aug. 2005, doi: 10.1016/j.energy.2004.08.018.
[33] Z. Jiancheng, H. Lipei, C. Zhiye, and W. Su, "Research on flywheel energy storage system for power quality," in *Proc. Int. Conf. Power Syst. Technol.*, vol. 1, Oct. 2002, pp. 496–499.
[34] A. Al-Diab and C. Sourkounis, "Unbalanced voltage drops compensations using flywheel energy storage system," in *Proc. 11th Int. Conf. Electr. Power Quality Utilisation*, Oct. 2011, pp. 1–6, doi: 10.1109/EPQU.2011.6128849.
[35] R. Peña-Alzola, R. Sebastián, J. Quesada, and A. Colmenar, "Review of flywheel based energy storage systems," in *Proc. Int. Conf. Power Eng., Energy Electr. Drives*, May 2011, pp. 1–6, doi: 10.1109/PowerEng.2011.6036455.
[36] M. Amiryar and K. Pullen, "A review of flywheel energy storage system technologies and their applications," *Appl. Sci.*, vol. 7, no. 3, p. 286, Mar. 2017, doi: 10.3390/app7030286.
[37] A. G. Olabi, T. Wilberforce, M. A. Abdelkareem, and M. Ramadan, "Critical review of flywheel energy storage system," *Energies*, vol. 14, no. 8, p. 2159, Apr. 2021, doi: 10.3390/en14082159.
[38] A. A. K. Arani, H. Karami, G. B. Gharehpetian, and M. S. A. Hejazi, "Review of flywheel energy storage systems structures and applications in power systems and microgrids," *Renew. Sustain. Energy Rev.*, vol. 69, pp. 9–18, Mar. 2017, doi: 10.1016/j.rser.2016.11.166.
[39] S. M. Mousavi G, F. Faraji, A. Majazi, and K. Al-Haddad, "A comprehensive review of flywheel energy storage system technology," *Renew. Sustain. Energy Rev.*, vol. 67, pp. 477–490, Jan. 2017, doi: 10.1016/j.rser.2016.09.060.
[40] J. W. Zhang, Y. H. Wang, G. C. Liu, and G. Z. Tian, "A review of control strategies for flywheel energy storage system and a case study with matrix converter," *Energy Rep.*, vol. 8, pp. 3948–3963, Nov. 2022, doi: 10.1016/j.egyr.2022.03.009.
[41] H. Liu and J. Jiang, "Flywheel energy storage—An upswing technology for energy sustainability," *Energy Buildings*, vol. 39, no. 5, pp. 599–604, May 2007, doi: 10.1016/j.enbuild.2006.10.001.
[42] D. Burley, "Theory and practice of confidentiality," *Nursing*, vol. 4, no. 41, pp. 23–24, Sep. 1991. [Online]. Available: http://www.ncbi.nlm.nih.gov/pubmed/1945108
[43] P. F. Ribeiro, B. K. Johnson, M. L. Crow, A. Arsoy, and Y. Liu, "Energy storage systems for advanced power applications," *Proc. IEEE*, vol. 89, no. 12, pp. 1744–1756, Dec. 2001, doi: 10.1109/5.975900.
[44] B. Bolund, H. Bernhoff, and M. Leijon, "Flywheel energy and power storage systems," *Renew. Sustain. Energy Rev.*, vol. 11, no. 2, pp. 235–258, Feb. 2007, doi: 10.1016/j.rser.2005.01.004.
[45] S. J. Amodeo, H. G. Chiacchiarini, and A. R. Oliva, "High-performance control of a DC–DC Z-source converter used for an excitation field driver," *IEEE Trans. Power Electron.*, vol. 27, no. 6, pp. 2947–2957, Jun. 2012, doi: 10.1109/TPEL.2011.2176751.
[46] G. Lei, J. Zhu, Y. Guo, C. Liu, and B. Ma, "A review of design optimization methods for electrical machines," *Energies*, vol. 10, no. 12, p. 1962, Nov. 2017, doi: 10.3390/en10121962.
[47] Z. Q. Zhu and D. Howe, "Electrical machines and drives for electric, hybrid, and fuel cell vehicles," *Proc. IEEE*, vol. 95, no. 4, pp. 746–765, Apr. 2007, doi: 10.1109/JPROC.2006.892482.
[48] W. Zhou, T. G. Habetler, and R. G. Harley, "Bearing condition monitoring methods for electric machines: A general review," in *Proc. IEEE Int. Symp. Diag. Electr. Mach., Power Electron. Drives*, Sep. 2007, pp. 3–6, doi: 10.1109/DEMPED.2007.4393062.
[49] R. J. Hayes, J. P. Kajs, R. C. Thompson, and J. H. Beno, "Design and testing of a flywheel battery for a transit bus," SAE Tech. Paper 1999-01-1159, 1999, doi: 10.4271/1999-01-1159.
[50] A. Emadi, A. Nasiri, and S. B. Bekiarov, *Uninterruptible Power Supplies and Active Filters*. Boca Raton, FL, USA: CRC Press, 2017, doi: 10.1201/9781420037869.
[51] M. Forouzesh, Y. P. Siwakoti, S. A. Gorji, F. Blaabjerg, and B. Lehman, "Step-up DC–DC converters: A comprehensive review of voltage-boosting techniques, topologies, and applications," *IEEE Trans. Power Electron.*, vol. 32, no. 12, pp. 9143–9178, Dec. 2017, doi: 10.1109/TPEL.2017.2652318.
[52] R. Takarli, M. Adib, A. Vahedi, and R. Beiranvand, "A bidirectional CLLC resonant converter for EV battery charger applications," in *Proc. 14th Power Electron., Drive Syst., Technol. Conf. (PEDSTC)*, Jan. 2023, pp. 1–6, doi: 10.1109/pedstc57673.2023.10087140.
[53] S. Xu and H. Wang, "Simulation and analysis of back-to-back PWM converter for flywheel energy storage system," in *Proc. 15th Int. Conf. Elect. Mach. Syst. (ICEMS)*, Oct. 2012, pp. 1–5.
[54] H. Akagi, "Large static converters for industry and utility applications," *Proc. IEEE*, vol. 89, no. 6, pp. 976–983, Jun. 2001, doi: 10.1109/5.931498.
[55] T. Dragicevic, S. Sucic, J. C. Vasquez, and J. M. Guerrero, "Flywheel-based distributed bus signalling strategy for the public fast charging station," *IEEE Trans. Smart Grid*, vol. 5, no. 6, pp. 2825–2835, Nov. 2014, doi: 10.1109/TSG.2014.2325963.
[56] S. Samineni, B. Johnson, H. Hess, and J. Law, "Modeling and analysis of a flywheel energy storage system with a power converter interface," in *Proc. Int. Conf. Power Syst. Transients (IPST)*, New Orleans, LA, USA, 2003, vol. 4, no. 1, pp. 1–6. [Online]. Available: https://www.ipstconf.org/papers/Proc_IPST2003/03IPST11b-03.pdf

[57] F. Díaz-González, F. D. Bianchi, A. Sumper, and O. Gomis-Bellmunt, "Control of a flywheel energy storage system for power smoothing in wind power plants," *IEEE Trans. Energy Convers.*, vol. 29, no. 1, pp. 204–214, Mar. 2014, doi: 10.1109/TEC.2013.2292495.

[58] H. Tarzamni, H. S. Gohari, M. Sabahi, and J. Kyyrä, "Non-isolated high step-up DC–DC converters: Comparative review and metrics applicability," *IEEE Trans. Power Electron.*, early access, Apr. 3, 2023, doi: 10.1109/TPEL.2023.3264172.

[59] X. Chang, Y. Li, W. Zhang, N. Wang, and W. Xue, "Active disturbance rejection control for a flywheel energy storage system," *IEEE Trans. Ind. Electron.*, vol. 62, no. 2, pp. 991–1001, Feb. 2015, doi: 10.1109/TIE.2014.2336607.

[60] R. S. Weissbach, G. G. Karady, and R. G. Farmer, "A combined uninterruptible power supply and dynamic voltage compensator using a flywheel energy storage system," *IEEE Trans. Power Del.*, vol. 16, no. 2, pp. 265–270, Apr. 2001, doi: 10.1109/61.915493.

[61] M. di Benedetto, A. Lidozzi, D. M. Kumar, H. K. Mudaliar, and M. Cirrincione, "Control strategy for flywheel energy storage systems on a three-level three-phase back-to-back converter," in *Proc. Int. Aegean Conf. Elect. Mach. Power Electron. (ACEMP), Int. Conf. Optim. Elect. Electron. Equip. (OPTIM)* Aug. 2019, pp. 372–376, doi: 10.1109/ACEMP-OPTIM44294.2019.9007161.

[62] G. O. Suvire, M. G. Molina, and P. E. Mercado, "Improving the integration of wind power generation into AC microgrids using flywheel energy storage," *IEEE Trans. Smart Grid*, vol. 3, no. 4, pp. 1945–1954, Dec. 2012, doi: 10.1109/TSG.2012.2208769.

[63] B. Wang and G. Venkataramanan, "Dynamic voltage restorer utilizing a matrix converter and flywheel energy storage," *IEEE Trans. Ind. Appl.*, vol. 45, no. 1, pp. 222–231, Feb. 2009, doi: 10.1109/TIA.2008.2009507.

[64] T. Friedli, J. W. Kolar, J. Rodriguez, and P. W. Wheeler, "Comparative evaluation of three-phase AC–AC matrix converter and voltage DC-link back-to-back converter systems," *IEEE Trans. Ind. Electron.*, vol. 59, no. 12, pp. 4487–4510, Dec. 2012, doi: 10.1109/TIE.2011.2179278.

[65] J. Zhang, L. Li, and D. G. Dorrell, "Control and applications of direct matrix converters: A review," *Chin. J. Electr. Eng.*, vol. 4, no. 2, pp. 18–27, Jun. 2018, doi: 10.23919/CJEE.2018.8409346.

[66] X. Liu, P. C. Loh, P. Wang, F. Blaabjerg, Y. Tang, and E. A. Al-Ammar, "Distributed generation using indirect matrix converter in reverse power mode," *IEEE Trans. Power Electron.*, vol. 28, no. 3, pp. 1072–1082, Mar. 2013, doi: 10.1109/TPEL.2012.2209205.

[67] E. Lee and K.-B. Lee, "Design and implementation of a reverse matrix converter for permanent magnet synchronous motor drives," *J. Electr. Eng. Technol.*, vol. 10, no. 6, pp. 2297–2306, Nov. 2015, doi: 10.5370/JEET.2015.10.6.2297.

[68] J. Zou, K. Liu, M. Zhao, and J. H. Hu, "Simulation of Flywheel Energy Storage System (FESS) using Z-source inverter," in *Proc. Int. Conf. Elect. Mach. Syst.*, Oct. 2010, pp. 266–269.

[69] W. Xian, L. Rui, F. Liang, S. Donglei, L. Dong, and S. Yi, "Application of energy storage technology in frequency control of high proportion new energy power system," in *Proc. 6th Asia Conf. Power Electr. Eng. (ACPEE)*, Apr. 2021, pp. 853–857, doi: 10.1109/ACPEE51499.2021.9437021.

[70] A. Elserougi, A. M. Massoud, and S. Ahmed, "Flywheel energy storage system based on boost DC–AC converter," in *Proc. IET Conf. Publications*, Sep. 2011, pp. 1–7, doi: 10.1049/cp.2011.0194.

[71] L. Wang, J. Y. Yu, and Y. T. Chen, "Dynamic stability improvement of an integrated offshore wind and marine-current farm using a flywheel energy-storage system," *IET Renewable Power Generation*, vol. 5, no. 5, pp. 387–396, 2011, doi: 10.1049/iet-rpg.2010.0194.

[72] M. S. Zarbil, A. Vahedi, H. A. Moghaddam, and M. Saeidi, "Design and implementation of flywheel energy storage system control with the ability to withstand measurement error," *J. Energy Storage*, vol. 33, Jan. 2021, Art. no. 102047, doi: 10.1016/j.est.2020.102047.

[73] T. D. Nguyen, G. Foo, K.-J. Tseng, and D. M. Vilathgamuwa, "Modeling and sensorless direct torque and flux control of a dual-airgap axial flux permanent-magnet machine with field-weakening operation," *IEEE/ASME Trans. Mechatronics*, vol. 19, no. 2, pp. 412–422, Apr. 2014, doi: 10.1109/TMECH.2013.2242481.

[74] G. O. Suvire and P. E. Mercado, "DSTATCOM with Flywheel Energy Storage System for wind energy applications: Control design and simulation," *Electr. Power Syst. Res.*, vol. 80, no. 3, pp. 345–353, Mar. 2010, doi: 10.1016/j.epsr.2009.09.020.

[75] G. O. Suvire and P. E. Mercado, "Active power control of a flywheel energy storage system for wind energy applications," *IET Renew. Power Gener.*, vol. 6, no. 1, pp. 9–16, 2012, doi: 10.1049/iet-rpg.2010.0155.

[76] M. Mansour, S. Bendoukha, N. Barhoumi, and M. F. Mimouni, "A comparative study of the speed control of an IM-based flywheel energy storage system using PI-DTC and RFOC strategies," *Int. J. Emerg. Electr. Power Syst.*, vol. 22, no. 1, pp. 73–83, Feb. 2021, doi: 10.1515/ijeeps-2020-0198.

[77] A. Soomro, M. E. Amiryar, K. R. Pullen, and D. Nankoo, "Comparison of performance and controlling schemes of synchronous and induction machines used in flywheel energy storage systems," *Energy Proc.*, vol. 151, pp. 100–110, Oct. 2018, doi: 10.1016/j.egypro.2018.09.034.

[78] X. Zhang and J. Yang, "A DC-link voltage fast control strategy for high-speed PMSM/G in flywheel energy storage system," *IEEE Trans. Ind. Appl.*, vol. 54, no. 2, pp. 1671–1679, Mar. 2018, doi: 10.1109/TIA.2017.2783330.

[79] X. Zhang and J. Yang, "A robust flywheel energy storage system discharge strategy for wide speed range operation," *IEEE Trans. Ind. Electron.*, vol. 64, no. 10, pp. 7862–7873, Oct. 2017, doi: 10.1109/TIE.2017.2694348.

[80] S. Talebi, B. Nikbakhtian, and H. A. Toliyat, "A novel algorithm for designing the PID controllers of high-speed flywheels for traction applications," in *Proc. IEEE Vehicle Power Propuls. Conf.*, Sep. 2007, pp. 574–579, doi: 10.1109/VPPC.2007.4544188.

[81] G. Cimuca, M. M. Radulescu, C. Saudemont, and B. Robyns. *DTC Versus FOC of an IM-based Flywheel Energy Storage System Associated to a Variable-Speed Wind Generator*. Accessed: Aug. 10, 2022. [Online]. Available: http://users.utcluj.ro/~cimuca/papers/electrimacs_2005.pdf

[82] A. Moualdia, A. Medjber, A. Kouzou, and O. Bouchhida, "DTC-SVPWM of an energy storage flywheel associated with a wind turbine based on the DFIM," *Scientia Iranica*, vol. 25, no. 6D, pp. 3532–3541, Dec. 2018, doi: 10.24200/sci.2017.4379.

[83] M. Ghasemi, A. Bagheri, M. Bongiorno, and J. R. Svensson, "A novel application of flywheel system to enhance fault-ride-through of the microgrids," in *Proc. Conf. Sustain. Energy Supply Energy Storage Syst.*, Sep. 2019, pp. 1–6.

[84] F. M. Borujeni and M. Ardebili, "DTC-SVM control strategy for induction machine based on indirect matrix converter in flywheel energy storage system," in *Proc. 6th Power Electron., Drive Syst. Technol. Conf. (PEDSTC)*, Feb. 2015, pp. 352–357, doi: 10.1109/PEDSTC.2015.7093300.

[85] L. Tziovani, L. Hadjidemetriou, C. Charalampous, M. Tziakouri, S. Timotheou, and E. Kyriakides, "Energy management and control of a flywheel storage system for peak shaving applications," *IEEE Trans. Smart Grid*, vol. 12, no. 5, pp. 4195–4207, Sep. 2021, doi: 10.1109/TSG.2021.3084814.

[86] P. Gamboa, S. Ferreira Pinto, J. Fernando Silva, and E. Margato, "A flywheel energy storage system with matrix converter controlled Permanent Magnet Synchronous Motor," in *Proc. 18th Int. Conf. Electr. Mach.*, Sep. 2008, pp. 1–5, doi: 10.1109/ICELMACH.2008.4799861.

[87] H. A. Moghaddam, O. Rezaei, A. Vahedi, M. Saeidi, and M. Ehsani, "A continuous control set of the model predictive controller of PMA-SynRM machine for high-performance flywheel energy storage system," *Int. J. Dyn. Control*, vol. 10, no. 5, pp. 1553–1566, Oct. 2022, doi: 10.1007/s40435-021-00907-z.

[88] T. Nguyen, K. Tseng, G. Foo, and S. Zhang, "Control of a dual-air-gap axial flux permanent magnet machine for a flywheel energy storage system: A model predictive control approach," *Austral. J. Electr. Electron. Eng.*, vol. 9, no. 4, pp. 401–410, 2012, doi: 10.1080/1448837X.2012.11464345.

[89] L. Leclercq, B. Robyns, and J. M. Grave, "Control based on fuzzy logic of a flywheel energy storage system associated with wind and diesel generators," *Math. Comput. Simul.*, vol. 63, nos. 3–5, pp. 271–280, Nov. 2003, doi: 10.1016/S0378-4754(03)00075-2.

[90] L. Leclercq, C. Saudemont, B. Robyns, G. Cimuca, and M. M. Radulescu, "Flywheel energy storage system to improve the integration of wind generators into a network," in *Proc. 5th Int. Symp. Adv. Electromech. Motion Syst.*, vol. 2, Nov. 2003, pp. 641–646.

[91] X. D. Sun, K. H. Koh, B. G. Yu, and M. Matsui, "Fuzzy-logic-based V/f control of an induction motor for a DC grid power-leveling system using flywheel energy storage equipment," *IEEE Trans. Ind. Electron.*, vol. 56, no. 8, pp. 3161–3168, Aug. 2009, doi: 10.1109/TIE.2009.2021679.

[92] L. Yin and Y. Li, "Fuzzy vector reinforcement learning algorithm for generation control of power systems considering flywheel energy storage," *Appl. Soft Comput.*, vol. 125, Aug. 2022, Art. no. 109149, doi: https://doi.org/10.1016/j.asoc.2022.109149.
[93] V. M. Jape, H. M. Suryawanshi, and J. P. Modak, "RETRACTED: An efficient grasshopper optimization with recurrent neural network controller-based induction motor to replace flywheel of the process machine," *Trans. Inst. Meas. Control*, vol. 43, no. 1, pp. 151–166, Aug. 2020, doi: 10.1177/0142331220938205.
[94] A. Abdel-Khalik, A. Elserougi, A. Massoud, and S. Ahmed, "A power control strategy for flywheel doubly-fed induction machine storage system using artificial neural network," *Electr. Power Syst. Res.*, vol. 96, pp. 267–276, Mar. 2013, doi: 10.1016/j.epsr.2012.11.012.
[95] Y. Feng, H. Lin, J. Yan, Y. Guo, and M. Huang, "A novel energy feedback control method of flywheel energy storage system based on radial basis function neural network," in *Proc. Int. Conf. Electr. Mach. Syst.*, Aug. 2011, pp. 1–4, doi: 10.1109/icems.2011.6073514.
[96] S. Gupta, S. Debnath, J. Laldingliana, and P. K. Biswas, "Analysis and simulation of fuzzy control base for single axis active magnetic bearing system," in *Proc. Int. Conf. Cutting-Edge Technol. Eng. (ICon-CuTE)*, Nov. 2019, pp. 131–135, doi: 10.1109/icon-cute47290.2019.8991527.
[97] W. Wang, Y. Li, M. Shi, and Y. Song, "Optimization and control of battery-flywheel compound energy storage system during an electric vehicle braking," *Energy*, vol. 226, Jul. 2021, Art. no. 120404, doi: 10.1016/j.energy.2021.120404.
[98] K. R. Pullen, "The status and future of flywheel energy storage," *Joule*, vol. 3, no. 6, pp. 1394–1399, Jun. 2019, doi: 10.1016/j.joule.2019.04.006.
[99] M. A. Khan, B. Asad, K. Kudelina, T. Vaimann, and A. Kallaste, "The bearing faults detection methods for electrical machines—The state of the art," *Energies*, vol. 16, no. 1, p. 296, Dec. 2022, doi: 10.3390/en16010296.
[100] P. P. Acarnley, B. C. Mecrow, J. S. Burdess, J. N. Fawcett, J. G. Kelly, and P. G. Dickinson, "Design principles for a flywheel energy store for road vehicles," *IEEE Trans. Ind. Appl.*, vol. 32, no. 6, pp. 1402–1408, Dec. 1996, doi: 10.1109/28.556644.
[101] Z. Long and Q. Zhiping, "Review of flywheel energy storage system," in *Proc. ISES World Congr.*, vols. 1–5. Berlin, Germany: Springer, 2008, pp. 2815–2819, doi: 10.1007/978-3-540-75997-3_568.
[102] J. R. Stack, T. G. Habetler, and R. G. Harley, "Fault classification and fault signature production for rolling element bearings in electric machines," in *Proc. 4th IEEE Int. Symp. Diag. Electr. Mach., Power Electron. Drives (SDEMPED)*, Aug. 2003, pp. 172–176, doi: 10.1109/DEMPED.2003.1234568.
[103] J. G. Bitterly, "Flywheel technology past, present, and 21st Century projections," in *Proc. 32nd Intersociety Energy Convers. Eng. Conf. (IECEC)*, Jul./Aug. 1997, pp. 2312–2315, doi: 10.1109/iecec.1997.658228.
[104] G. G. Sotelo, R. de Andrade, and A. C. Ferreira, "Magnetic bearing sets for a flywheel system," *IEEE Trans. Appl. Supercond.*, vol. 17, no. 2, pp. 2150–2153, Jun. 2007, doi: 10.1109/TASC.2007.899268.
[105] H. Bleuler, J. Sandtner, Y.-J. Regamey, and F. Barrot, "Passive magnetic bearings for flywheels," in *Proc. Int. Symp. Magn. Suspension Technol.*, Sep. 2005, pp. 1–12. [Online]. Available: https://www.researchgate.net/publication/228554073_Passive_Magnetic_Bearings_for_Flywheels
[106] R. de Andrade, G. G. Sotelo, A. C. Ferreira, L. G. B. Rolim, J. L. da Silva Neto, R. M. Stephan, W. I. Suemitsu, and R. Nicolsky, "Flywheel energy storage system description and tests," *IEEE Trans. Appl. Supercond.*, vol. 17, no. 2, pp. 2154–2157, Jun. 2007, doi: 10.1109/TASC.2007.899056.
[107] A. V. Filatov and E. H. Maslen, "Passive magnetic bearing for flywheel energy storage systems," *IEEE Trans. Magn.*, vol. 37, no. 6, pp. 3913–3924, Nov. 2001, doi: 10.1109/20.966127.
[108] M. I. Daoud, A. S. Abdel-Khalik, A. Massoud, S. Ahmed, and N. H. Abbasy, "On the development of flywheel storage systems for power system applications: A survey," in *Proc. 20th Int. Conf. Electr. Mach.*, Sep. 2012, pp. 2119–2125, doi: 10.1109/ICElMach.2012.6350175.
[109] S. O. Siems, W.-R. Canders, H. Walter, and J. Bock, "Superconducting magnetic bearings for a 2 MW/10 kW h class energy storage flywheel system," *Superconductor Sci. Technol.*, vol. 17, no. 5, pp. S229–S233, May 2004, doi: 10.1088/0953-2048/17/5/027.
[110] M. Ren, Y. Shen, Z. Li, and K. Nonami, "Modeling and control of a flywheel energy storage system using active magnetic bearing for vehicle," in *Proc. Int. Conf. Inf. Eng. Comput. Sci. (ICIECS)*, Dec. 2009, pp. 1–5, doi: 10.1109/ICIECS.2009.5364972.
[111] H. Gotanda, R. Amano, and T. Sugiura, "Mode coupling of a flexible rotor supported by a superconducting magnetic bearing due to the nonlinearity of electromagnetic force," *IEEE Trans. Appl. Supercond.*, vol. 21, no. 3, pp. 1481–1484, Jun. 2011, doi: 10.1109/TASC.2010.2096791.
[112] X. Yanliang, D. Yueqin, W. Xiuhe, and K. Yu, "Analysis of hybrid magnetic bearing with a permanent magnet in the rotor by FEM," *IEEE Trans. Magn.*, vol. 42, no. 4, pp. 1363–1366, Apr. 2006, doi: 10.1109/TMAG.2006.871396.
[113] S. Sivrioglu and K. Nonami, "Active permanent magnet support for a superconducting magnetic-bearing flywheel rotor," *IEEE Trans. Appl. Supercond.*, vol. 10, no. 4, pp. 1673–1677, Dec. 2000, doi: 10.1109/77.913142.
[114] C. Zhang and K. Jet Tseng, "A novel flywheel energy storage system with partially-self-bearing flywheel-rotor," *IEEE Trans. Energy Convers.*, vol. 22, no. 2, pp. 477–487, Jun. 2007, doi: 10.1109/TEC.2005.858088.
[115] M. Subkhan and M. Komori, "New concept for flywheel energy storage system using SMB and PMB," *IEEE Trans. Appl. Supercond.*, vol. 21, no. 3, pp. 1485–1488, Jun. 2011, doi: 10.1109/TASC.2010.2098470.
[116] M. Strasik, P. E. Johnson, A. C. Day, J. Mittleider, M. D. Higgins, J. Edwards, J. R. Schindler, K. E. McCrary, C. R. McIver, D. Carlson, J. F. Gonder, and J. R. Hull, "Design, fabrication, and test of a 5-kWh/100-kW flywheel energy storage utilizing a high-temperature superconducting bearing," *IEEE Trans. Appl. Supercond.*, vol. 17, no. 2, pp. 2133–2137, Jun. 2007, doi: 10.1109/TASC.2007.898065.
[117] A. Cansiz, I. Yildizer, E. A. Oral, and Y. Kaya, "An effective noncontact torque mechanism and design considerations for an evershed-type superconducting magnetic bearing system," *IEEE Trans. Appl. Supercond.*, vol. 24, no. 1, pp. 22–29, Feb. 2014, doi: 10.1109/TASC.2013.2280033.
[118] A. Lanzon and P. Tsiotras, "A combined application of H_∞ loop shaping and μ-synthesis to control high-speed flywheels," *IEEE Trans. Control Syst. Technol.*, vol. 13, no. 5, pp. 766–777, Sep. 2005, doi: 10.1109/TCST.2005.847344.
[119] Z. Kohari, V. Tihanyi, and I. Vajda, "Loss evaluation and simulation of superconducting magnetic bearings," *IEEE Trans. Appl. Supercond.*, vol. 15, no. 2, pp. 2328–2331, Jun. 2005, doi: 10.1109/TASC.2005.849644.
[120] J. R. Fang, L. Z. Lin, L. G. Yan, and L. Y. Xiao, "A new flywheel energy storage system using hybrid superconducting magnetic bearings," *IEEE Trans. Appl. Supercond.*, vol. 11, no. 1, pp. 1657–1660, Mar. 2001, doi: 10.1109/77.920099.
[121] X. Li, B. Anvari, A. Palazzolo, Z. Wang, and H. Toliyat, "A utility-scale flywheel energy storage system with a shaftless, hubless, high-strength steel rotor," *IEEE Trans. Ind. Electron.*, vol. 65, no. 8, pp. 6667–6675, Aug. 2018, doi: 10.1109/TIE.2017.2772205.
[122] R. Östergård, "Flywheel energy storage: A conceptual study," M.S. thesis, Dept. Eng. Sci., Uppsala Univ., Uppsala, Sweden, 2011.
[123] I. Boldea and S. A. Nasar, *The Induction Machines Design Handbook*. Boca Raton, FL, USA: CRC Press, 2018, doi: 10.1201/9781315222592.
[124] K. Kumar, M. Marchesoni, Z. Maule, M. Passalacqua, F. Soso, and L. Vaccaro, "Currents and torque oscillations mitigation in high power induction motor drives," in *Proc. IEEE 15th Int. Conf. Compat., Power Electron. Power Eng. (CPE-POWERENG)*, Jul. 2021, pp. 1–5, doi: 10.1109/CPE-POWERENG50821.2021.9501186.
[125] J. Yang, C. Ye, and S. Huang, "Development and analysis of an outer rotor homopolar inductor machine for flywheel energy storage system," *IEEE Trans. Ind. Electron.*, vol. 68, no. 8, pp. 6504–6515, Aug. 2021, doi: 10.1109/TIE.2020.3005107.
[126] A. Soomro, M. E. Amiryar, D. Nankoo, and K. R. Pullen, "Performance and loss analysis of squirrel cage induction machine based flywheel energy storage system," *Appl. Sci.*, vol. 9, no. 21, p. 4537, Oct. 2019, doi: 10.3390/app9214537.
[127] J. Wu, J. Wen, and H. Sun, "A new energy storage system based on flywheel," in *Proc. IEEE Power Energy Soc. Gen. Meeting*, Jul. 2009, pp. 1–6, doi: 10.1109/PES.2009.5275460.
[128] S.-Y. Hahn, W.-S. Kim, J. Hoon Kim, C.-S. Koh, and S.-Y. Hahn, "Low speed FES with induction motor and generator," *IEEE Trans. Appl. Supercond.*, vol. 12, no. 1, pp. 746–749, Mar. 2002, doi: 10.1109/TASC.2002.1018509.

[129] L. Ran, D. Xiang, and J. L. Kirtley, "Analysis of electromechanical interactions in a flywheel system with a doubly fed induction machine," *IEEE Trans. Ind. Appl.*, vol. 47, no. 3, pp. 1498–1506, May 2011, doi: 10.1109/TIA.2011.2127436.

[130] I. Alan and T. A. Lipo, "Induction machine based flywheel energy storage system," *IEEE Trans. Aerosp. Electron. Syst.*, vol. 39, no. 1, pp. 151–163, Jan. 2003, doi: 10.1109/TAES.2003.1188900.

[131] M. A. Awadallah and B. Venkatesh, "Energy storage in flywheels: An overview," *Can. J. Electr. Comput. Eng.*, vol. 38, no. 2, pp. 183–193, Spring. 2015, doi: 10.1109/CJECE.2015.2420995.

[132] S. Ahmadi and A. Vahedi, "Rotor design of IPMSM traction motor based on multi-objective optimization using BFGS method and train motion equations," *Iranian J. Elect. Electron. Eng.*, vol. 11, no. 3, pp. 217–221, Sep. 2015. [Online]. Available: http://ijeee.iust.ac.ir/article-1-770-en.html

[133] A. Serpi, F. Deiana, G. Gatto, and I. Marongiu, "Performance analysis of PMSM for high-speed flywheel energy storage systems in electric and hybrid electric vehicles," in *Proc. IEEE Int. Electr. Vehicle Conf. (IEVC)*, Dec. 2014, pp. 1–8, doi: 10.1109/IEVC.2014.7056202.

[134] B. Anvari, X. Li, H. A. Toliyat, and A. Palazzolo, "A coreless permanent-magnet machine for a magnetically levitated shaft-less flywheel," *IEEE Trans. Ind. Appl.*, vol. 54, no. 5, pp. 4288–4296, Sep. 2018, doi: 10.1109/TIA.2018.2839747.

[135] J.-P. Lee, B.-J. Park, Y.-H. Han, S.-Y. Jung, and T.-H. Sung, "Energy loss by drag force of superconductor flywheel energy storage system with permanent magnet rotor," *IEEE Trans. Magn.*, vol. 44, no. 11, pp. 4397–4400, Nov. 2008, doi: 10.1109/TMAG.2008.2002633.

[136] R. Arghandeh, M. Pipattanasomporn, and S. Rahman, "Flywheel energy storage systems for ride-through applications in a facility microgrid," *IEEE Trans. Smart Grid*, vol. 3, no. 4, pp. 1955–1962, Dec. 2012, doi: 10.1109/TSG.2012.2212468.

[137] B. H. Kenny, P. E. Kascak, R. Jansen, T. Dever, and W. Santiago, "Control of a high-speed flywheel system for energy storage in space applications," *IEEE Trans. Ind. Appl.*, vol. 41, no. 4, pp. 1029–1038, Aug. 2005, doi: 10.1109/TIA.2005.851021.

[138] H. Lee, B. Y. Shin, S. Han, S. Jung, B. Park, and G. Jang, "Compensation for the power fluctuation of the large scale wind farm using hybrid energy storage applications," *IEEE Trans. Appl. Supercond.*, vol. 22, no. 3, Jun. 2012, Art. no. 5701904, doi: 10.1109/TASC.2011.2180881.

[139] D.-J. You, S.-M. Jang, J.-P. Lee, and T.-H. Sung, "Dynamic performance estimation of high-power FESS using the operating torque of a PM synchronous motor/generator," *IEEE Trans. Magn.*, vol. 44, no. 11, pp. 4155–4158, Nov. 2008, doi: 10.1109/TMAG.2008.2002607.

[140] D. Gerada, A. Mebarki, N. L. Brown, C. Gerada, A. Cavagnino, and A. Boglietti, "High-speed electrical machines: Technologies, trends, and developments," *IEEE Trans. Ind. Electron.*, vol. 61, no. 6, pp. 2946–2959, Jun. 2014, doi: 10.1109/TIE.2013.2286777.

[141] A. S. Nagorny, N. V. Dravid, R. H. Jansen, and B. H. Kenny, "Design aspects of a high speed permanent magnet synchronous motor/generator for flywheel applications," in *Proc. IEEE Int. Conf. Electr. Mach. Drives*, May 2005, pp. 635–641, doi: 10.1109/IEMDC.2005.195790.

[142] V. Korsunskiy, "Simulation model of a transport vehicle with a fixed-ratio transmission and a flywheel energy storage in case of random external action," *IOP Conf. Ser., Mater. Sci. Eng.*, vol. 820, no. 1, Apr. 2020, Art. no. 012015, doi: 10.1088/1757-899X/820/1/012015.

[143] S.-M. Jang, D.-J. You, K.-J. Ko, and S.-K. Choi, "Design and experimental evaluation of synchronous machine without iron loss using double-sided Halbach magnetized PM rotor in high power FESS," *IEEE Trans. Magn.*, vol. 44, no. 11, pp. 4337–4340, Nov. 2008, doi: 10.1109/TMAG.2008.2001499.

[144] J.-H. Choi, S.-M. Jang, S.-Y. Sung, J.-M. Kim, Y.-S. Park, Y.-J. Kim, and D.-H. Oh, "Operating range evaluation of double-side permanent magnet synchronous motor/generator for flywheel energy storage system," *IEEE Trans. Magn.*, vol. 49, no. 7, pp. 4076–4079, Jul. 2013, doi: 10.1109/TMAG.2013.2239273.

[145] M. M. Flynn, "A methodology for evaluating and reducing rotor losses, heating, and operational limitations of high-speed flywheel batteries," Ph.D. Thesis, Dept. Elect. Comput. Eng., Univ. Texas, Austin, TX, USA, 2003. Accessed: Aug. 10, 2022. [Online]. Available: http://hdl.handle.net/2152/11987

[146] K.-H. Kim, H.-I. Park, S.-M. Jang, and J.-Y. Choi, "Comparison of characteristics of double-sided permanent-magnet synchronous motor/generator according to magnetization patterns for flywheel energy storage system using an analytical method," *IEEE Trans. Magn.*, vol. 51, no. 3, pp. 1–4, Mar. 2015, doi: 10.1109/TMAG.2014.2358791.

[147] R. Cardenas, R. Pena, M. Perez, J. Clare, G. Asher, and P. Wheeler, "Power smoothing using a flywheel driven by a switched reluctance machine," *IEEE Trans. Ind. Electron.*, vol. 53, no. 4, pp. 1086–1093, Jun. 2006, doi: 10.1109/TIE.2006.878325.

[148] E. Bernsmüller, L. G. B. Rolim, and A. C. Ferreira, "External rotor switched reluctance machine for a kinetic energy storage system," in *Proc. 42nd Annu. Conf. IEEE Ind. Electron. Soc.*, Oct. 2016, pp. 1636–1641, doi: 10.1109/IECON.2016.7793958.

[149] K. Vijayakumar, R. Karthikeyan, S. Paramasivam, R. Arumugam, and K. N. Srinivas, "Switched reluctance motor modeling, design, simulation, and analysis: A comprehensive review," *IEEE Trans. Magn.*, vol. 44, no. 12, pp. 4605–4617, Dec. 2008, doi: 10.1109/TMAG.2008.2003334.

[150] R. Rocca, S. Papadopoulos, M. Rashed, G. Prassinos, F. G. Capponi, and M. Galea, "A one-body, laminated-rotor flywheel switched reluctance machine for energy storage: Design trade-offs," in *Proc. IEEE Int. Conf. Environ. Elect. Eng., IEEE Ind. and Commercial Power Syst. Eur. (EEEIC/I&CPS Europe)*, Jun. 2020, pp. 1–6, doi: 10.1109/EEEIC/ICPSEurope49358.2020.9160512.

[151] X. Sun, Z. Jin, S. Wang, Z. Yang, K. Li, Y. Fan, and L. Chen, "Performance improvement of torque and suspension force for a novel five-phase BFSPM machine for flywheel energy storage systems," *IEEE Trans. Appl. Supercond.*, vol. 29, no. 2, pp. 1–5, Mar. 2019, doi: 10.1109/TASC.2019.2893295.

[152] Z. Zhu, J. Wang, and M. Cheng, "A novel axial split phase bearingless flywheel machine with hybrid-inner-stator permanent magnet-based structure," *IEEE Trans. Energy Convers.*, vol. 36, no. 3, pp. 1873–1882, Sep. 2021, doi: 10.1109/TEC.2020.3045143.

[153] J.-D. Park, C. Kalev, and H. F. Hofmann, "Control of high-speed solid-rotor synchronous reluctance motor/generator for flywheel-based uninterruptible power supplies," *IEEE Trans. Ind. Electron.*, vol. 55, no. 8, pp. 3038–3046, Aug. 2008, doi: 10.1109/TIE.2008.918583.

[154] C.-Y. Ho, J.-C. Wang, K.-W. Hu, and C.-M. Liaw, "Development and operation control of a switched-reluctance motor driven flywheel," *IEEE Trans. Power Electron.*, vol. 34, no. 1, pp. 526–537, Jan. 2019, doi: 10.1109/TPEL.2018.2814790.

[155] G. F. Lukman, K.-I. Jeong, and J.-W. Ahn, "Pole selection of switched reluctance machine for FESS," in *Proc. IEEE 5th Student Conf. Electr. Mach. Syst. (SCEMS)*, Nov. 2022, pp. 1–4, doi: 10.1109/scems56272.2022.9990789.

[156] T. M. G. Vieira, J. G. Oliveira, L. A. Almeida, G. G. Sotelo, M. V. Coutinho, and G. L. Ferreira, "Switched reluctance machine in a flywheel energy storage system for grid applications," in *Proc. Simposio Brasileiro Sistemas Eletricos (SBSE)*, May 2018, pp. 1–6, doi: 10.1109/sbse.2018.8395780.

[157] H. A. Moghaddam, A. Vahedi, and S. H. Ebrahimi, "Design optimization of transversely laminated synchronous reluctance machine for flywheel energy storage system using response surface methodology," *IEEE Trans. Ind. Electron.*, vol. 64, no. 12, pp. 9748–9757, Dec. 2017, doi: 10.1109/TIE.2017.2716877.

[158] X. B. Bomela and M. J. Kamper, "Effect of stator chording and rotor skewing on performance of reluctance synchronous machine," *IEEE Trans. Ind. Appl.*, vol. 38, no. 1, pp. 91–100, Feb. 2002, doi: 10.1109/28.980362.

[159] A. Fratta, G. P. Troglia, A. Vagati, and F. Villata, "Evaluation of torque ripple in high performance synchronous reluctance machines," in *Proc. Conf. Rec. IEEE Ind. Appl. Conf., 28th IAS Annu. Meeting*, vol. 1, Oct. 1993, pp. 163–170, doi: 10.1109/ias.1993.298919.

[160] W. Zhang, L. Cheng, and H. Zhu, "Suspension force error source analysis and multidimensional dynamic model for a centripetal force type-magnetic bearing," *IEEE Trans. Ind. Electron.*, vol. 67, no. 9, pp. 7617–7628, Sep. 2020, doi: 10.1109/TIE.2019.2946568.

[161] W. Zhang, H. Yang, L. Cheng, and H. Zhu, "Modeling based on exact segmentation of magnetic field for a centripetal force type-magnetic bearing," *IEEE Trans. Ind. Electron.*, vol. 67, no. 9, pp. 7691–7701, Sep. 2020, doi: 10.1109/TIE.2019.2945275.

[162] X. Sun, B. Su, S. Wang, Z. Yang, G. Lei, J. Zhu, and Y. Guo, "Performance analysis of suspension force and torque in an IBPMSM with V-shaped PMs for flywheel batteries," *IEEE Trans. Magn.*, vol. 54, no. 11, pp. 1–4, Nov. 2018, doi: 10.1109/TMAG.2018.2827103.

[163] F. Yang, Y. Yuan, G. Meng, and L. Yan, "Design and analysis of a high-integration and low-loss bearingless flywheel motor in vehicle," *Electron. Lett.*, vol. 57, no. 10, pp. 390–392, May 2021, doi: 10.1049/ell2.12006.

[164] Y. Yuan, Y. Sun, and Y. Huang, "Design and analysis of bearingless flywheel motor specially for flywheel energy storage," *Electron. Lett.*, vol. 52, no. 1, pp. 66–68, Jan. 2016, doi: 10.1049/el.2015.1938.
[165] Y. Yuan, Y. Sun, and Y. Huang, "Radial force dynamic current compensation method of single winding bearingless flywheel motor," *IET Power Electron.*, vol. 8, no. 7, pp. 1224–1229, Jul. 2015, doi: 10.1049/iet-pel.2014.0502.
[166] M. Ooshima, S. Kobayashi, and H. Tanaka, "Magnetic suspension performance of a bearingless motor/generator for flywheel energy storage systems," in *Proc. IEEE PES Gen. Meeting*, Jul. 2010, pp. 1–4, doi: 10.1109/PES.2010.5589783.
[167] Y. Liu, H. Zhu, and B. Xu, "Mathematical modelling and control of bearingless brushless direct current machine with motor and generator double modes for flywheel battery," *IET Power Electron.*, vol. 15, no. 13, pp. 1249–1263, Apr. 2022, doi: 10.1049/pel2.12295.
[168] Y. Sun, F. Yang, Y. Yuan, and Y. Huang, "Out rotor bearingless brushless DC motor for flywheel energy storage," in *Proc. Int. Workshop Complex Syst. Netw. (IWCSN)*, Dec. 2017, pp. 7–12, doi: 10.1109/IWCSN.2017.8276496.
[169] M. Strasik, P. E. Johnson, A. C. Day, J. Mittleider, M. D. Higgins, J. Edwards, J. R. Schindler, K. E. McCrary, C. R. McIver, D. Carlson, J. F. Gonder, and J. R. Hull, "Design, fabrication, and test of a 5-kWh/100-kW flywheel energy storage utilizing a high-temperature superconducting bearing," *IEEE Trans. Appl. Supercond.*, vol. 17, no. 2, pp. 2133–2137, Jun. 2007, doi: 10.1109/TASC.2007.898065.
[170] S. R. Gurumurthy, V. Agarwal, and A. Sharma, "Optimal energy harvesting from a high-speed brushless DC generator-based flywheel energy storage system," *IET Electr. Power Appl.*, vol. 7, no. 9, pp. 693–700, Nov. 2013, doi: 10.1049/iet-epa.2013.0134.
[171] M. Baszynski and S. Pirog, "A novel speed measurement method for a high-speed BLDC motor based on the signals from the rotor position sensor," *IEEE Trans. Ind. Informat.*, vol. 10, no. 1, pp. 84–91, Feb. 2014, doi: 10.1109/TII.2013.2243740.
[172] G. Liu and C. Zhang, "Sliding mode control of reaction flywheel-based brushless DC motor with buck converter," *Chin. J. Aeronaut.*, vol. 26, no. 4, pp. 967–975, Aug. 2013, doi: 10.1016/j.cja.2013.04.038.
[173] K. Liu, M. Yin, W. Hua, Z. Ma, M. Lin, and Y. Kong, "Design and optimization of an external rotor ironless BLDCM used in a flywheel energy storage system," *IEEE Trans. Magn.*, vol. 54, no. 11, pp. 1–5, Nov. 2018, doi: 10.1109/TMAG.2018.2837098.
[174] E. Severson, R. Nilssen, T. Undeland, and N. Mohan, "Magnetic equivalent circuit modeling of the AC homopolar machine for flywheel energy storage," *IEEE Trans. Energy Convers.*, vol. 30, no. 4, pp. 1670–1678, Dec. 2015, doi: 10.1109/TEC.2015.2441040.
[175] F. Jiancheng, W. Xi, W. Tong, T. Enqiong, and F. Yahong, "Homopolar 2-pole radial permanent-magnet biased magnetic bearing with low rotating loss," *IEEE Trans. Magn.*, vol. 48, no. 8, pp. 2293–2303, Aug. 2012, doi: 10.1109/TMAG.2012.2192131.
[176] E. Severson, R. Nilssen, T. Undeland, and N. Mohan, "Suspension force model for bearingless AC homopolar machines designed for flywheel energy storage," in *Proc. 7th IEEE GCC Conf. Exhib. (GCC)*, Nov. 2013, pp. 274–279, doi: 10.1109/IEEEGCC.2013.6705789.
[177] P. Tsao, M. Senesky, and S. Sanders, "A synchronous homopolar machine for high-speed applications," in *Proc. Conf. Rec. IEEE Ind. Appl. Conf., 37th IAS Annu. Meeting*, vol. 1, Oct. 2002, pp. 406–416, doi: 10.1109/ias.2002.1044119.
[178] P. Tsao, M. Senesky, and S. R. Sanders, "An integrated flywheel energy storage system with homopolar inductor motor/generator and high-frequency drive," *IEEE Trans. Ind. Appl.*, vol. 39, no. 6, pp. 1710–1725, Dec. 2003, doi: 10.1109/TIA.2003.818992.
[179] G.-R. Duan, Z.-Y. Wu, C. Bingham, and D. Howe, "Robust magnetic bearing control using stabilizing dynamical compensators," *IEEE Trans. Ind. Appl.*, vol. 36, no. 6, pp. 1654–1660, Dec. 2000, doi: 10.1109/28.887218.
[180] E. Severson, R. Nilssen, T. Undeland, and N. Mohan, "Outer-rotor ac homopolar motors for flywheel energy storage," in *Proc. 7th IET Int. Conf. Power Electron., Mach. Drives (PEMD)*, Apr. 2014, pp. 1–6.
[181] W. Li, K. T. Chau, T. W. Ching, Y. Wang, and M. Chen, "Design of a high-speed superconducting bearingless machine for flywheel energy storage systems," *IEEE Trans. Appl. Supercond.*, vol. 25, no. 3, pp. 1–4, Jun. 2015, doi: 10.1109/TASC.2014.2367008.
[182] K. Davey, A. Filatov, and R. Thompson, "Design and analysis of passive homopolar null flux bearings," *IEEE Trans. Magn.*, vol. 41, no. 3, pp. 1169–1175, Mar. 2005, doi: 10.1109/TMAG.2004.841703.
[183] C. Ye, J. Yang, F. Xiong, and Z. Q. Zhu, "Relationship between homopolar inductor machine and wound-field synchronous machine," *IEEE Trans. Ind. Electron.*, vol. 67, no. 2, pp. 919–930, Feb. 2020, doi: 10.1109/TIE.2019.2898577.
[184] Q. Wang, C. Liu, J. Zou, X. Fu, and J. Zhang, "Numerical analysis and design optimization of a homopolar inductor machine used for flywheel energy storage," *IEEE Trans. Plasma Sci.*, vol. 41, no. 5, pp. 1290–1294, May 2013, doi: 10.1109/TPS.2013.2243847.
[185] C. Ye, K. Yu, W. Xu, and H. Zhang, "Optimal design and experimental research of a capacitor-charging pulsed alternator," *IEEE Trans. Energy Convers.*, vol. 30, no. 3, pp. 948–956, Sep. 2015, doi: 10.1109/TEC.2015.2395446.
[186] C. Ye, J. Yang, W. Xu, F. Xiong, and X. Liang, "A novel multi-unit out-rotor homopolar inductor machine for flywheel energy storage system," *IEEE Trans. Magn.*, vol. 54, no. 11, pp. 1–5, Nov. 2018, doi: 10.1109/TMAG.2018.2834956.
[187] (2022). *Neodymium Iron Boron Magnets*. Accessed: Aug. 10, 2022. [Online]. Available: https://www.arnoldmagnetics.com/products/neodymium-iron-boron-magnets/
[188] S. S. R. Bonthu, M. T. B. Tarek, and S. Choi, "Optimal torque ripple reduction technique for outer rotor permanent magnet synchronous reluctance motors," *IEEE Trans. Energy Convers.*, vol. 33, no. 3, pp. 1184–1192, Sep. 2018, doi: 10.1109/TEC.2017.2781259.
[189] Y. Wang, G. Bacco, and N. Bianchi, "Geometry analysis and optimization of PM-assisted reluctance motors," *IEEE Trans. Ind. Appl.*, vol. 53, no. 5, pp. 4338–4347, Sep. 2017, doi: 10.1109/TIA.2017.2702111.
[190] R.-R. Moghaddam and F. Gyllensten, "Novel high-performance SynRM design method: An easy approach for a complicated rotor topology," *IEEE Trans. Ind. Electron.*, vol. 61, no. 9, pp. 5058–5065, Sep. 2014, doi: 10.1109/TIE.2013.2271601.
[191] N. Bianchi, E. Fornasiero, and W. Soong, "Selection of PM flux linkage for maximum low-speed torque rating in a PM-assisted synchronous reluctance machine," *IEEE Trans. Ind. Appl.*, vol. 51, no. 5, pp. 3600–3608, Sep. 2015, doi: 10.1109/TIA.2015.2416236.
[192] H. Heidari, A. Rassőlkin, A. Kallaste, T. Vaimann, E. Andriushchenko, A. Belahcen, and D. V. Lukichev, "A review of synchronous reluctance motor-drive advancements," *Sustainability*, vol. 13, no. 2, p. 729, Jan. 2021, doi: 10.3390/su13020729.
[193] (2022). *Alibaba Company*. Accessed: Jul. 27, 2022. [Online]. Available: https://www.alibaba.com/
[194] (2022). *The London Metal Exchange is the World Centre for the Trading of Industrial Metals*. Accessed: Jul. 27, 2022. [Online]. Available: https://www.lme.com/en/
[195] Y. Wang, N. Bianchi, and R. Qu, "Comparative study of non-rare-earth and rare-earth PM motors for EV applications," *Energies*, vol. 15, no. 8, p. 2711, Apr. 2022, doi: 10.3390/en15082711.
[196] H. Ibrahim, A. Ilinca, and J. Perron, "Energy storage systems—Characteristics and comparisons," *Renew. Sustain. Energy Rev.*, vol. 12, no. 5, pp. 1221–1250, Jun. 2008, doi: 10.1016/j.rser.2007.01.023.
[197] A. Nobahari, A. Vahedi, and R. Nasiri-Zarandi, "A modified permanent magnet-assisted synchronous reluctance motor design for torque characteristics improvement," *IEEE Trans. Energy Convers.*, vol. 37, no. 2, pp. 989–998, Jun. 2022, doi: 10.1109/TEC.2021.3127081.

REZA TAKARLI (Student Member, IEEE) was born in Hamedan, Iran, in 1998. He received the B.Sc. degree in electrical engineering from the Faculty of Electrical Engineering, Bu-Ali Sina University (BASU), Hamedan, in 2020. He is currently pursuing the M.Sc. degree in electrical engineering with the Department of Electrical Engineering, Iran University of Science and Technology, Tehran, Iran. His current research interests include power electronic converters analysis and design, soft-switching and resonant converters, high step-up power conversion, electric vehicles, and energy storage systems. He was a recipient of the "Distinguished Master Student Award" from the Iran University of Science and Technology (IUST), from 2020 to 2021.

ALI AMINI was born in Isfahan, Iran, in 1997. He received the B.Sc. degree in electrical engineering from the Faculty of Electrical Engineering, Yazd University, Yazd, Iran, in 2019. He is currently pursuing the M.Sc. degree (Hons.) in electrical engineering with the Department of Electrical Engineering, Iran University of Science and Technology (IUST), Tehran, Iran. His current research interests include wireless power transfer and performing finite element analysis (FEA), reliability analysis, multi-objective optimization, and the design of electrical machines.

MOHAMMADSADEGH KHAJUEEZADEH was born in Kerman, Iran, in 1996. He received the M.Sc. degree (Hons.) in electrical engineering from the Department of Electrical Engineering, Sharif University of Technology, Tehran, Iran, in 2021. He is currently a Research Assistant (RA) with the Special Machines and Drives (SEMD) Laboratory, Iran University of Science and Technology (IUST). His current research interests include performing finite element analysis (FEA), reliability analysis, vibration analysis, and artificial intelligence (AI)-based fault diagnosis of electrical machines and electromagnetic sensors.

MOHAMMAD SHADNAM ZARBIL was born in Kaleybar, East Azerbaijan, Iran, in 1990. He received the B.S. degree (Hons.) in electrical power engineering from Azarbaijan Shahid Madani University, Tabriz, Iran, in 2013, and the M.S. degree in electrical power engineering (power electronics and systems) from the University of Tabriz, Tabriz, in 2015. He is currently pursuing the Ph.D. degree with the Department of Electrical Power Engineering (Power Electronics and Drive), Iran University of Science and Technology, Tehran, Iran. His current research interests include power electronics, electric machine drive, energy storage, and electric vehicle.

ABOLFAZL VAHEDI (Senior Member, IEEE) was born in Tehran, Iran, in 1966. He received the B.S. degree in electrical engineering from the Ferdowsi University of Mashhad, Iran, in 1989, and the M.Sc. and Ph.D. degrees in electrical engineering from the Institut National Polytechnique de Lorraine, Nancy, France, in 1992 and 1996, respectively. He is currently a Professor with the Department of Electrical Engineering, Iran University of Science and Technology, Tehran, where he is the Head of the Special Machines and Drives Laboratory. His current research interests include design, modeling, optimization, and fault detection of electric machines and drives.

ARASH KIYOUMARSI was born in Shahr-e-Kord, Iran, in September 1972. He received the B.Sc. degree (Hons.) in electronics engineering from the Petroleum University of Technology (PUT), Iran, in 1995, and the M.Sc. and Ph.D. degrees (Hons.) in electrical power engineering from the Isfahan University of Technology (IUT), Iran, in 1998 and 2004, respectively.

In March 2005, he joined the Department of Electrical Engineering, Faculty of Engineering, University of Isfahan, as an Assistant Professor of electrical machines. From February 2006 to October 2006 and from July 2007 to August 2007, he was a Postdoctoral Research Fellow with the Alexander-von-Humboldt (AvH) Foundation, Institute of Electrical Machines, Technical University of Berlin. In March 2012, he became an Associate Professor of electrical machines with the Department of Electrical Engineering, Faculty of Engineering, University of Isfahan. In July 2014, he was a Visiting Guest Professor with the Institute of Electrical Machines, RWTH Aachen University, as a Research Fellow of the AvH Foundation. From April 2017 to September 2017, he was a Guest Professor with the Department of Electrical and Computer Engineering, University of Manitoba, Winnipeg, Canada. Then, he was a Visiting Guest Professor as a Research Fellow with the AvH Foundation, Institute of Electrical Energy Conversion (IEW), Faculty of Computer Science, Electrical Engineering and Information Technology, University of Stuttgart, from July 2019 to September 2019. His research interests include the application of time-stepping finite element analysis in electromagnetic and electrical machines, interior permanent-magnet synchronous motor-drive, and the design and analysis of electrical machines.

Dr. Kiyoumarsi was a recipient of the Best Teachers' Award from the University of Isfahan, in 2013.

HADI TARZAMNI (Student Member, IEEE) was born in Tabriz, Iran, in 1992. He received the B.Sc. and M.Sc. degrees (Hons.) in power electrical engineering from the Faculty of Electrical and Computer Engineering, University of Tabriz, Tabriz, in 2014 and 2016, respectively. He is currently pursuing the dual Ph.D. degree in power electronics engineering with the School of Electrical Engineering, Sharif University of Technology, Tehran, Iran, and the Department of Electrical Engineering and Automation, Aalto University, Espoo, Finland. He has authored and coauthored more than 35 journal and conference papers. He also holds six patents in the area of power electronics. Since January 2021, he has been a Researcher with the Department of Electrical Engineering and Automation and the Department of Electronics and Nanoengineering, Aalto University, Finland. His research interests include power electronic converters analysis and design, dc–dc and dc–ac converters, high step-up power conversion, soft-switching and resonant converters, and reliability analysis. He was a recipient of the Best Paper Award from the 10th International Power Electronics, Drive Systems and Technologies Conference (PEDSTC), in 2019. He has been awarded a three-year Aalto ELEC Doctoral School grant, and a Jenny and Antti Wihuri Foundation Grant, in 2021 and 2022, respectively.

JORMA KYYRA (Member, IEEE) received the M.Sc., Lic.Sc., and D.Sc. degrees from the Helsinki University of Technology (TKK), which is now Aalto University, Helsinki, Finland, in 1987, 1991, and 1995, respectively.

Since 1985, he has been with the university in various positions. Since 1996, he has been an Associate Professor of power electronics. Since 1998, he has also been a Professor of power electronics. From 2008 to 2009, he was the Dean of the Faculty of Electronics, Communications and Automation, TKK. From 2009 to 2011, he was the Vice President of Aalto University, Espoo, Finland, where he is currently the Head of the Department of Electrical Engineering and Automation. The power electronics group at Aalto University has expertise, such as in power electronics for ac drives, dc–dc converters, modeling of converters, filtering of EMI, power factor correction, and distributed power systems. His research interest includes power electronics at large.